



HAL
open science

Use of hydraulic tests at different scales to characterize fracture network properties in the weathered-fractured layer of a hard rock aquifer

Jean-Christophe Maréchal, Benoît Dewandel, K. Subrahmanyam

► **To cite this version:**

Jean-Christophe Maréchal, Benoît Dewandel, K. Subrahmanyam. Use of hydraulic tests at different scales to characterize fracture network properties in the weathered-fractured layer of a hard rock aquifer. *Water Resources Research*, 2004, 40, pp.W11508. 10.1029/2004WR003137 . hal-00458384

HAL Id: hal-00458384

<https://hal.science/hal-00458384>

Submitted on 21 Feb 2010

HAL is a multi-disciplinary open access archive for the deposit and dissemination of scientific research documents, whether they are published or not. The documents may come from teaching and research institutions in France or abroad, or from public or private research centers.

L'archive ouverte pluridisciplinaire **HAL**, est destinée au dépôt et à la diffusion de documents scientifiques de niveau recherche, publiés ou non, émanant des établissements d'enseignement et de recherche français ou étrangers, des laboratoires publics ou privés.

Use of hydraulic tests at different scales to characterize fracture network properties in the weathered-fractured layer of a hard rock aquifer

J.C. Maréchal^{a,b*}, B. Dewandel^a, K. Subrahmanyam^c

^a brgm (bureau de recherches géologiques et minières), WATER Department, Indo-French Centre for Groundwater Research, NGRI, Uppal Road, 500 007 Hyderabad, India

^b Now: brgm (bureau de recherches géologiques et minières), WATER Department, 1039 rue de Pinville, 34 000 Montpellier, France

^c National Geophysical Research Institute, Indo-French Center for Groundwater Research, Uppal Road, 500 007 Hyderabad, India

* Correspondence : Bureau de Recherches Géologiques et Minières, WATER Department, 1039 rue de Pinville, 34 000 Montpellier, France, Tel: + 33 4 67 15 79 68, Fax: + 33 4 67 15 79 75, jc.marechal@brgm.fr

Abstract

The hydrodynamic properties of the weathered-fractured layer of a hard-rock pilot watershed in a granitic terrain are characterized using hydraulic tests at different scales. The interpretation of numerous slug tests leads to characterize the statistical distribution of local permeabilities in the wells. The application of flowmeter profiles during injection tests determines the vertical distribution of conductive fracture zones and their permeabilities. It appears that the extension of the most conductive part of the weathered-fractured layer is limited down to 35 meters depth. The partition of drainage porosity between blocks (90%) and fractures (10%) is determined thanks to the interpretation of pumping tests using a double porosity model. The application of anisotropic and single fracture analytical solutions on pumping test data allows to determine, respectively, the degree of anisotropy of permeability ($K_r/K_z = 10$) and the radius (4 to 16 meters) of the horizontal conductive fractures crossed by the wells. Two different scales of fractures networks are identified: the primary fracture network (PFN), which affects the matrix on a decimeter scale by contributing to an increase in the permeability and storage capacity of the blocks, and the secondary fracture network (SFN), which affects the blocks at the borehole scale. SFN is composed of two sets of fractures. The main set of horizontal fractures is responsible for the sub-horizontal permeability of the weathered-fractured layer. A second set of less permeable sub-vertical fractures insures the connectivity of the aquifer at the borehole scale. The good connectivity of fractures networks is shown by fractional dimension flow solutions. The absence of scale effect in the study area suggests that the hydraulic conductivity at the borehole scale is laterally homogeneous. Finally, the analysis and synthesis of the hydrodynamic properties allow to propose a comprehensive hydrodynamic model of the fractured-weathered layer. Many geological and hydrogeological indicators suggest that a continuous and laterally homogeneous weathering process is responsible for the origin of the fractures and permeability encountered in the aquifer. These results confirm the major role played by weathering in the origin of fractures and on resulting hydrodynamic parameters in the shallow part of hard-rock aquifers.

Index Terms

5104 - Fracture and flow, 5114 - Permeability and porosity, 1829 - Groundwater hydrology, 9320 - Asia, 1886 - Weathering (1625)

Key words

Hard rock and granite, pumping test, India, hydraulic conductivity, fracture, anisotropy

1. INTRODUCTION

Hard rocks and their associated aquifers occur in many areas of the world. They are principally (but not always) exposed in large areas called shields, composed mainly of metamorphic and magmatic rocks of Precambrian or Archean ages, and form the most tectonically stable parts of the continents. The importance of hard-rock aquifers for hydrogeological and water management issues differs from place to place, depending on various factors, but mainly on the overall availability of water and the water demand. In arid and semi-arid regions, due to the lack of surface water resources, special attention has traditionally been paid to shallow groundwater. The existence of semi-arid or arid climates in hard-rock regions increases the interest by hydrogeologists for such aquifers namely in Africa, Brazil or India (Gustafson and Krasny, 1994). India, with hard rock constituting more than two-thirds of the total surface, is a great example of the nexus between water scarcity and the occurrence of hard-rock aquifers. The groundwater boom during the Green revolution of the seventies has led to a complete inversion of the irrigation scenario, with groundwater now sustaining almost 60 % of irrigated land (Roy and Shah, 2002). As recently pointed out by Bredehoeft (2002), sustainable groundwater development of an aquifer usually depends on the dynamic response of the system to development. The principal tool to evaluate the sustainability of management scenarios for hydrosystems is groundwater modeling. One of the major prerequisites for establishing the reliability of such models is an accurate knowledge of the geometry and the hydrodynamic properties of the aquifer.

Hard-rock aquifers generally occupy the upper tens of meters of the subsurface profile (Detay et al., 1989). The hydrogeological characteristics (e.g., hydraulic conductivity and storage) of the weathered mantle and underlying bedrock derive primarily from the geomorphologic processes of deep weathering and erosion (Taylor and Howard, 2000; Wyns et al., 2004). The classical weathering profile (see Figure 1) is composed of the following layers (from top to bottom), which have specific hydrodynamic properties:

- Unconsolidated weathered mantle (saprolite or regolith), with a thickness from negligible to a few tens of meters, derived from prolonged *in-situ* decomposition of bedrock. Usually, this unconsolidated layer has a high porosity and a low permeability (Acworth, 1987). When saturated, this layer constitutes the reservoir of the aquifer;
- Fractured-weathered layer, generally characterized by a fracture density that decreases with depth (Houston and Lewis, 1988; Howard et al., 1992). These fractures could be caused by cooling stresses in the magma, subsequent tectonic activity (Houston and Lewis, 1988) or lithostatic decompression processes (Davis and Turk, 1964; Acworth, 1987; Wright, 1992). Recent works (Lachassagne et al., 2001; Wyns et al., 2004) demonstrate that they also result from the weathering process itself. This layer mainly assumes the transmissive function in the aquifer and is pumped by most of the wells drilled in hard-rock areas;
- Fresh basement, which is permeable only locally where deep tectonic fractures are present. This deep part of the hard-rock aquifers has been investigated in numerous countries

(Canada, England, Finland, Sweden, Switzerland, United States) under various nuclear waste disposal programs (Blomqvist, 1990; Walker et al., 2001; Pickens et al., 1987) and is not the subject of this paper, which focuses on the shallow aquifers of hard-rock.

Given that the unconsolidated weathered mantle can be represented by a porous medium, its hydrodynamic properties can be easily measured *in-situ* and many data (see, for instance, Acworth, 1987) are available for modeling. On the other hand, due to the heterogeneity, discontinuity and anisotropy induced by the fracture networks, the hydrogeology of the fractured-weathered layer is more complex. The scientific community has long focused on the specific capacities (Summers, 1972) or yields of wells in crystalline rocks as a function of their depth (Davis and Turk, 1964), geology (Houston and Lewis, 1988) or weathering profile (Foster, 1984). Many authors have studied the evolution with depth of the transmissivity and the storage in the upper part of the weathered crystalline basement (Chilton and Foster, 1984). The optimization of the location of boreholes in tectonically fractured areas using geophysics (Barker et al., 1992; White et al., 1988), remote sensing (Sander, 1997; Mabee and Hardcastle, 1997) or geological data (Houston and Lewis, 1988) has been a major issue for rural water supplies, namely in Africa (Chilton and Smith-Carington, 1984). More recently, Taylor and Howard (2000) have proposed a tectono-geomorphic model of the hydrogeology of crystalline rock from Uganda, and have pointed out the shallow hydrogeology of such rocks in relation to their geological context. Most of these studies cite transmissivity estimates of the fractured zone of weathered crystalline rocks without considering the total hydrodynamic behavior of the layer or the relationships between fracture networks and the rock matrix. Other related properties such as anisotropy, connectivity or distribution of storage between matrix and fractures are not explored. Therefore, there was a need to apply existing interpretation techniques specific to fractured media in order to propose a conceptual model of the geometry and physics of water flow in the weathered-fractured layer of hard-rock aquifers.

2. METHODOLOGY AND STUDY AREA

Extensive fieldwork has been carried out on a hard-rock aquifer in India (Maheshwaram watershed). Hydraulic tests at different investigation scales were used to determine the hydrodynamic properties of the weathered-fractured layer. Slug tests, injection tests, flowmeter tests, and pumping tests are interpreted using specific techniques for fractured media. Hydraulic conductivity, storage coefficient, anisotropy, connectivity, fracture density, conductivity and radius of the fractures are investigated using various analytical solutions (Table 1).

First, the interpretation of numerous slug tests in observation wells allows to get information on the statistical distribution of local permeabilities (§ 3). The application of flowmeter profiles during injection tests locates in depth zones of fractures and their permeabilities, including the vertical density of fractures (§ 3). Pumping tests are then interpreted using a double porosity model in order to determine the respective contribution of blocks and fractures to storage coefficient and hydraulic conductivity (§ 4). The application of anisotropic and single fracture analytical solutions allows to determine, respectively, the degree of anisotropy of permeability and the radius of conductive horizontal fractures crossed by the wells (§ 5). Then, connectivity of fractures networks is explored using fractional dimension flow solutions (§ 6). Except flowmeter profiles and injection tests, the results are interpreted using transient analytical solutions in order to improve the analysis precision. Both unconfined and confined solutions are used; this point will be justified later (§ 5). The scale effect is characterized comparing previous results of various tests at different scales

(§ 7). Finally, the analysis and synthesis of the hydrodynamic properties introduce a hydrodynamic model of the fractured-weathered layer (§ 8).

The Maheshwaram watershed is composed mainly of Archean granites. The surface of the watershed, located around the village of Maheshwaram 30 kilometers from Hyderabad (Andhra Pradesh, India), is about 55 km² (Figure 2a). The major part of the basin is constituted by biotite granite (centimetric grain-size) often including porphyritic K-feldspars. Leucogranites are observed in the southwestern part of the basin. The weathering profile is observable from numerous dugwells previously used by the farmers for irrigation (Figure 2b). The weathering profile is generally truncated by erosion; overlain by a few decimeters of red soil, the weathered mantle has quite a homogeneous thickness of less than three meters throughout the watershed. A high density of sub-horizontal fractures is observed in the underlying fractured-weathered layer. A few sub-vertical fractures are also present. This layer is estimated from borewells observations (from cuttings) to be between 20 and 40 meters thick. Due to the over-exploitation of groundwater resources, water levels are far below ground level; thus, the weathered mantle is dry and only the deeper weathered-fractured layer is saturated. This feature was used to carry out hydraulic tests with the objective of characterizing the hydrodynamic properties of the weathered-fractured layer only.

A series of 34 observation wells were drilled in the watershed to depths ranging from 32 to 45 meters (Figure 2a). The absence of a confining layer and the storage values obtained from hydraulic tests suggest that the aquifer is unconfined. The frequent observation during drilling that the final static water level lies above the level at which water is initially encountered is explained by the separation of the fracture systems into discrete flow horizons by low-permeability blocks.

3. LOCAL HYDRAULIC CONDUCTIVITY AND VERTICAL DISTRIBUTION OF FRACTURES

Thirty slug tests were achieved in the wells and interpreted using the Bouwer and Rice (1976) technique for unconfined aquifers with completely or partially penetrating wells. The distribution of hydraulic conductivity obtained (Table 2) constitutes a preliminary estimate of the hydraulic conductivity of the fractured-weathered layer in close proximity to the well. The values range from 2×10^{-8} m/s up to 5×10^{-4} m/s and exhibit a near-lognormal distribution with a geometric mean of 4.4×10^{-6} m/s (Figure 3a). Within this distribution, a small population of three boreholes (IFP-5, IFP-19 and IFP-25) with permeabilities of less than 10^{-7} m/s corresponds to the less fractured granite.

The location of hydraulically conductive fractures was obtained using vertical profiles of flowmeter measurements. Given that pumping induces drawdown of water level in the well, it decreases the thickness of the zone where flows take place. In order to increase the vertical extension of the investigated zone where flowmeter measurements can be done, the experiment was made during injection and not pumping. During injection at constant rate, after a pseudo-steady state had been reached, the flowmeter, which measures the vertical flow within the screened portion of the well, was lowered almost to the bottom of the well and a measurement of the velocity was obtained. Velocity measurements were taken every 0.5 m. The final result is a series of data points giving the vertical discharge within the screen as a function of depth.

As is usually assumed (Molz et al., 1989), the aquifer is considered as a series of horizontal layers. The difference between two successive meter readings constitutes the net radial flow (q_i) entering each layer of the aquifer. Then, the Dupuit (1848, 1863) formula for horizontal flow to a well in a confined aquifer is applied to each layer, leading to an estimation of the layer hydraulic conductivity:

$$K_i = \frac{q_i}{2\pi s} \ln \frac{R_i}{r_w}$$

with

K_i = the conductivity of the i^{th} layer;
 s = the drawdown;
 R_i = the radius of influence;
 r_w = the well radius.

A correction factor is applied to the obtained conductivities in order that the total conductivity of the well calculated from the sum of the layer conductivities (according to the principle of parallel layers: $K = \sum K_i$) is equal to the total conductivity obtained by applying the Dupuit (1848, 1863) formula for an unconfined aquifer to the injection test results:

$$K = \frac{Q}{\pi s(2s + b)} \ln \frac{R_i}{r_w}$$

with

b = initial saturated thickness of aquifer;
 Q = the total injection flow.

Seventeen tests were conducted in the most permeable observation wells according to the sensitivity of the flowmeter, the total injection flow during the test being higher than 25 l/min. In the absence of core samples in such a fractured aquifer, it is not possible to determine if the identified conductive layers (which ones where the net radial flow is not nil) are constituted by a single fracture, several fractures or a fractured zone. Therefore, in order to avoid any confusion, the results are referred to “conductive fractures zones (CFZ)” without any hypothesis concerning their exact nature (single fracture, multi-fractures...). According to the geometry of the well and the observed drawdowns, the sensitivity of the flowmeter limits the identification of fractures zones to those with a hydraulic conductivity higher than 1×10^{-5} m/s (hydraulic transmissivity $T > 5 \times 10^{-6}$ m²/s), corresponding to a net radial flow of about 5.5 l/m/min in a 0.5 meter-thick layer. This means that the technique gives information only on the most conductive fractures zones. This is illustrated in Figure 3b where the distribution of permeability in the conductive fracture zones is assumed to be lognormal, even though information on the low-permeability conductive fracture zones is not available. The geometric mean of available data is $K_{CFZ} = 8.8 \times 10^{-5}$ m/s.

The vertical profile of fracture zones distribution (Figure 4a) shows the occurrence of conductive fractures between 9 and 39.5 meters, with higher concentrations of fractures between 15 and 30 meters. However, observations are limited at shallow depths by the presence of unperforated casings in the boreholes, and by the bottom of the well at deeper depths. Thus, it is necessary in the interpretation to consider a statistical bias of the data introduced by unequal representation of the depth ranges for the investigated boreholes. The curve on Figure 4b shows that observations between 15 and 42 meters can be considered as representative, the percentage of investigated wells being higher than 50 % (for a given aquifer portion, ratio between the number of available observations and the total 17 possible measurements, Figure 4b). The low number of observations at shallow depths (down to 15 meters) suggests that the apparent decrease in fractures density above 15 meters is an artifact due to a lack of observations (ratio decreasing much, Figure 4b). Consequently, it can reasonably be assumed that the weathered-fractured layer extends above the upper limit of observations, which is consistent with field and well geological observations.

The bottom of the weathered-fractured layer is better constrained thanks to the quality of the available observations. The number of fractures starts to decrease between 30 and 35 meters (Figure 4a) and is followed by an absence of fractures below 35 meters while the quality ratio of observations remains high down to 39 meters (Figure 4b). This depth roughly

corresponds to the top of the fresh basement as identified by geological observations during the drilling of the wells, and also to a sudden decrease in drilling rates at this depth. Figure 4c shows a profile of the arithmetic average of the hydraulic conductivities (including those less than 1×10^{-5} m/s, which are considered nil) obtained from flowmeters for each 0.5 meter-thick layer in all tested wells. It demonstrates the effect of the number of fractures on hydraulic conductivity, with the more highly transmissive zone located mainly between 9 and 35 meters. These observations mean that in the watershed area the weathered-fractured layer has a limited vertical extent (e.g., from the bottom of the weathered mantle down to maximum 35 meters depth).

For each well, the vertical density of the fracture zones is the ratio of the number of conductive fracture zones to the thickness of the investigated weathered-fractured layer (equal to the difference between the final water level during the injection test and the bottom of the weathered-fractured layer as defined above). The density varies from 0.04 conductive fracture zones per meter in IFP-11/3, where only one conductive fracture zone was identified, up to 1.10 fractures per meter in IFP-16, where 27 conductive fracture zones were detected. While slug and injection tests investigate the full range of permeability, flowmeter tests could be done only in wells with a total permeability in the range of 5.0×10^{-7} m/s up to 2.0×10^{-4} m/s. Thus, there is a lack of information for low-permeability wells with few fractures or with only low-permeability fractures. Consequently, the density of conductive fracture zones obtained from flowmeter measurements is estimated from a biased data set and cannot be extrapolated to the entire data set. Therefore, we are able only to determine a range for the CFZ density according to the following hypothesis. As shown below (§ 4), the three borewells (IFP-5, IFP-19 and IFP-25 on Figure 2a) with the lowest permeability were drilled in an unfractured block of granite; it is assumed that their CFZ density is zero. This solves the problem for only the three wells concerned. The results of the other wells - where no flowmeter test could be done because of the low total permeability, but where a single conductive fracture might be present - can be interpreted in two ways, introducing a range of values for the average density. (1) Neglecting these in the calculation of CFZ density will lead to its overestimation by up to 0.24 m^{-1} . (2) On the other hand, considering that they don't intersect any CFZ (e.g., assuming a nil density in these wells too impermeable for a flowmeter measurement) will underestimate the density by as much as 0.15 m^{-1} . The true value is comprised between these two limits. This range of density of conductive fracture zones in such a weathered-fractured layer leads to a vertical persistence (e.g., the distance between two consecutive CFZ, equal to the inverse of the density) between 4.2 and 6.8 meters. Figure 5 shows a regular increase of hydraulic conductivities for slug and injection tests with the density of CFZ intersected by the wells. This suggests that the total permeability of the aquifer is controlled mainly by the density of CFZ. As suggested by the absence of wells in the low-density of CFZ – high-conductivity zone (shaded triangle on Figure 5), a highly permeable well does not correspond to one single very conductive fracture zone, but to the presence of several contributing fracture zones characterized by similar permeability values.

As illustrated by photograph on Figure 2b and its interpretation, outcrop observations in dugwells suggest that the fractures intersected by the wells are mainly sub-horizontal. The distribution, anisotropy and connectivity of the fractures and their relationships to the blocks control the flow in the weathered-fractured layer making the interpretation of pumping tests using the classical Theis method difficult. No universal method exists to interpret pumping tests in fractured media, but the literature provides a package of specific methods that can reveal different aspects of the hydrodynamic properties of such aquifers (Maréchal et al., 2003a). These are applied below to available data using the information on the fracture distribution, providing a set of valuable information on the fractured layer.

4. DOUBLE POROSITY

Five long-duration pumping tests were conducted in five IFP wells located in the watershed (Figure 2a). Another pumping test conducted by the Andhra Pradesh Groundwater Department in the same weathered-fractured media (well BD9) a few kilometers away from the basin was also interpreted in order to increase the statistical significance of the results. Table 3 summarizes the characteristics of the tests.

The vertical distribution of CFZ show the existence between identified conductive fractures of blocks with a mean vertical thickness estimated between 4.2 and 6.8 meters. The double-porosity model (DP model), also known as the ‘overlapping continua’ or ‘double continuum’, was originally proposed by Barenblatt and Zheltov (1960) and Barenblatt et al. (1960). In this conceptual model, the fractured porous medium domain is represented by two distinct, but interacting, subsystems: one consisting of a network of fractures and the other, of the porous blocks. Each subsystem is conceptualized as a continuum occupying the entire investigated domain. Interaction phenomena between the two continua include the exchange of fluid between fractures and porous blocks, as described by Bear (1993) for a pumping test at a constant rate:

- i. Initially, fluid is removed primarily from the fractures, as a consequence of the much higher permeability of the fractures than of the porous blocks. During this phase, a straight line is obtained when the pressure decline in a well producing at a constant rate is plotted against the logarithm of time.
- ii. Gradually, flow at an increasing rate takes place from the porous blocks to the fractures. This appears as a curve of variable slope on the above plot and a U-shaped curve on the log-plot of the drawdown derivative (note that the “U” of derivatives can often be masked by well effects if they last for a long time).
- iii. Then equilibrium is reached between the two continua. This appears on the above plot as a straight line having the same slope as that describing the pressure decline during the initial period, but now the line is displaced parallel to the previous one. This indicates that the entire fractured porous rock behaves as an equivalent, single, homogeneous continuum. The equality of the slopes during the first and third stages indicates that the permeability in the latter is primarily that of the fractures.

In the Warren and Root (1963) double-porosity model, each system occupies the entire investigated domain and is characterized by its own hydrodynamic properties: K_f and S_f are the permeability and the storage coefficient of the fracture medium, respectively, and K_b and S_b are the permeability and the storage coefficient of the blocks, respectively. In a confined aquifer of thickness H , the flow radial to the pumping well is controlled only by the transmissivity of the fractures (flow from the blocks to the pumping well is nil, $K_f \gg K_b$) and the fracture network drains the blocks in which the flow is stationary (spatial variation of the hydraulic head is neglected). Two main parameters characterize the geometry of fractures and blocks: N (entire and dimensionless) is the number of orthogonal fracture sets ($N = 1, 2$ or 3); l is the width of a block (or persistence).

This method is illustrated at pumping well IFP-16. The derivatives of drawdowns (derivatives with respect of logarithm of times, $ds/d(\ln t)$) in IFP-16 have a shape typical of a double-porosity aquifer (Figures 6a & 6b):

- i. well effects and flow through fractures to pumping well;
- ii. transitional period: the “U” illustrates the contribution of the block flow through fractures to the pumping; and
- iii. flow in fractures and block.

The ‘U’ shape of the derivatives curve suggests that the application of the Warren and Root method is then justified for this data set (Figure 6b). For the interpretation based on the flowmeter measurements, the value $l=0.9$ meters was used for this well. The best matching of the observations was obtained with $N=2$. The hydraulic conductivity of the fracture network appears to be $K_f = 5.9 \times 10^{-5}$ m/s and that of the block is $K_b = 2.6 \times 10^{-7}$ m/s. On Figure 6a is also presented the interpretation using the Theis method, which cannot be properly model the drawdown after 470 minutes of pumping.

The results of the application of this model to all the pumping tests are summarized in Table 4. The fracture network commonly used to match the observed data is a horizontal fracture set cross-cut by a vertical one ($N = 2$), suggesting the existence of a network complementary to the horizontal one as observed in the dugwells. The (geometric) mean of the hydraulic conductivity of the fracture network is 2.1×10^{-5} m/s, 400 times higher than that of the blocks (i.e. 5.1×10^{-8} m/s). This last value is similar to the lowest of the hydraulic conductivities estimated from slug-tests (Table 1). These low values were measured in three wells IFP-5, IFP-19 and IFP-25 on Figure 3a, suggesting that these wells were drilled in an unfractured area where only the hydraulic conductivity of the blocks contributes to the flow. However, it is quite probable that a primary network of fractures (PFN) also affects the matrix, accounting for the high value of the hydraulic conductivity (10^{-8} m/s) of the blocks compared to those measured on rock samples of the same lithology (matrix permeability $K_m = 10^{-9} - 10^{-14}$ m/s, de Marsily, 1986). At this stage, the use of the term “primary” refers only to the small scale (block-level) of the fracture network and does not imply any consideration on the specific origin of the PFN. That point will be considered in the final discussion. Together, the horizontal and the vertical sets of fractures observed in dugwells and designated in the double-porosity model constitute the secondary fracture network (SFN) at the borehole scale. The total storage coefficient (specific yield in this unconfined aquifer, obtained from the sum of fracture and block storage coefficients) is equal to 6.3×10^{-3} , a value quite consistent with those evaluated from other interpretation methods: Neuman technique (see § 5) or the water-table fluctuation techniques (Maréchal et al., 2003b). Storage in the primary fractures network (PFN) affecting the matrix accounts for the bulk (91 %) of the total storage of the aquifer; the secondary fracture network (SFN) contributes the rest (9 %).

5. VERTICAL ANISOTROPY

In order to characterize the anisotropy induced by the horizontal set of the secondary fracture network (HSFN) observed in the dugwells (Figure 2b), drawdowns in observation wells were interpreted by the Neuman method (1975) while drawdowns in the pumping wells were analyzed using the theory of the horizontal fracture developed by Gringarten and Witherspoon (1972).

Neuman method for the observation wells

On a log-log plot (Figure 7), the drawdown curves for the observation wells IFP-1/1 and IFP-1/2 during pumping tests at IFP-1 have a complex shape which is difficult to interpret with classical methods, even considering an impermeable boundary. Drawdown curves are composed of three segments: an initial segment with a steep slope for a short time after the start, followed by an intermediate period during which the slope stabilizes, and a final segment the slope of which again steeping after a long time.

This theory, initially developed by Boulton (1970), integrates the notion of “delayed yield from storage in unconfined aquifers” (Boulton and Pontin, 1971). It was improved by

Neuman (1972, 1975) who developed an analytical solution adapted to anisotropic unconfined aquifers, where K_r is the radial horizontal permeability and K_z is the vertical permeability. The Neuman model (anisotropic (AN) model) considers an infinite unconfined homogeneous aquifer. When a completed well is pumped at a constant discharge rate, one part of the water comes from the storage in the aquifer and the other, from gravitational drainage at the free surface. The Neuman solution, plotted on type curves, provides reduced drawdowns in an observation well located at a radial distance r from the pumping well,

$$s_{DN} = \frac{4\pi Ts}{Q} \text{ as a function of:}$$

- Reduced time $t_s = \frac{Tt}{Sr^2}$ for a series of “type A” curves;
- Reduced time $t_y = \frac{Tt}{S_y r^2}$ for a series of “type B” curves;

with

- $T =$ the transmissivity of the aquifer;
- $S =$ the (elastic) storage coefficient;
- $S_y =$ the specific yield;
- $t =$ the time since the start of pumping; and
- $s =$ the drawdown.

The application of this method consists in matching the observed drawdowns on the abacus for the two types of curves: a type-A curve for short times and a type-B curve for late times (Figure 7). Both curves are characterized by the same parameter $\beta = \frac{r^2 K_D}{b^2}$, where the permeability anisotropy is $K_D = \frac{K_z}{K_r}$ and b the thickness of the aquifer.

The application of this method (Table 5) to the observation wells leads to the evaluation of transmissivities (T), storage coefficients (S) and specific yields (S_y). Very similar values obtained in each observation well for T_A and T_B (transmissivity corresponding to curves A and B, respectively) show the coherence of the interpretation of these pumping tests using Neuman method.

In accordance with geological observations, the interpretation of the data from the observation wells (Table 6) arises an anisotropy of the permeability tensor: the horizontal permeability is systematically higher (9 times on average) than the vertical. This result is consistent with the observation of many horizontal fractures in dugwells (Maréchal et al., 2003c). The average value of the vertical permeability ($K_z = 1.3 \times 10^{-6}$ m/s) is much higher than the permeability of the blocks obtained from the application of the double-porosity model. This confirms that the second set of sub-vertical fractures belonging to the secondary fracture network (VSFN) is less permeable than the horizontal and that it also affects the entire aquifer by ensuring its vertical permeability and drainage.

The advantage of the Neuman technique is the ability to determine both specific yield and elastic storage coefficient. The values obtained for the specific yield ($S_y = 5 \times 10^{-3}$ as an average) are consistent with an unconfined aquifer of low drainage porosity, as also suggested by water-table fluctuations analysis at the watershed scale (Maréchal et al., 2003b). The storage coefficient ($S = 5 \times 10^{-4}$) is one order of magnitude lower than the specific yield. Because the observed drawdowns are most of the times low (< 25%) compared to the thickness of the aquifer, the application of analytical solutions for confined aquifer to the unconfined aquifer of the study area is possible without introducing any inaccuracy. This is

confirmed by the comparison between the values obtained for specific yields and hydraulic conductivity (Figure 8) using double porosity model (confined aquifer solution) and anisotropic model (unconfined aquifer solution). The difference between the average values is less than 30% for both parameters, which is very low compared to uncertainties usually existing in the determination of storage and permeability. Consequently, although the aquifer is clearly unconfined, a few techniques for confined aquifers, are applied in this study.

Gringarten method for pumping wells

The vertical flowmeter profiles for wells IFP-1 and IFP-9 (Figure 9) demonstrate that these wells intersect few conductive fracture zones: three CFZ (F1/1, F1/2 and F1/3) for the former and one CFZ (F9/1) for the latter. Actually, for IFP-1, only the deepest CFZ (F1/3 at 31.5 meters) was saturated during the whole pumping test. The low hydraulic-head losses estimated using the Jacob method (Jacob, 1945) for the step test suggest the desaturation of F1/1 and F1/2. In IFP-9, the only intersected CFZ (F9/1 at 29 meters) was also saturated during the whole pumping test. Moreover, analysis by the Neuman method documents the existence of hydraulic anisotropy due to the presence of horizontal fractures. Thus, the method developed by Gringarten and Ramey (1974) for a vertical well intersecting a horizontal fracture (single-fracture (SF) model) in an anisotropic aquifer, applicable to a pumping well, is well adapted to the hydrogeological context of IFP-1 and IFP-9 wells.

The analytical solution requires an interpretation through the adjustment of observed drawdowns on theoretical type curves (Gringarten and Witherspoon, 1972) resulting in reduced drawdowns (s_{DG}) in a pumping well as a function of reduced time (t_{DG}) for various geometrical configurations represented by the parameter H_{DG} . When the fracture is located at the center of the aquifer ($z_f/H = 0.5$),

where

$$t_{DG} = \frac{K_r t}{S_s r_f^2}$$

$$s_{DG} = \frac{4\pi \sqrt{K_r K_z} r_f s}{Q} \text{ and}$$

$$H_{DG} = \frac{H}{r_f} \sqrt{\frac{K_r}{K_z}}.$$

and

- z_f = the distance between the fracture and the bottom of the aquifer;
- H = the aquifer thickness;
- K_r = the permeability in the radial direction parallel to the fracture, (which can be interpreted as the permeability increased by the existence of the horizontal fracture)
- K_z = the vertical permeability (which represents the block permeability);
- S_s = the specific storage coefficient;
- t = the time since the start of pumping;
- r_f = the radius of the horizontal fracture;
- s = the drawdown; and
- Q = the pumping rate.

Adjustments of observed drawdowns by the Gringarten theoretical curves lead to high values of H_{DG} , suggesting a high permeability anisotropy. The hydrodynamic properties have

been evaluated only for the conductive fractures (Table 7), based on a knowledge of the geometry of the aquifer in each case (i.e. the thickness H of the aquifer), and the application of the anisotropy ratio value, K_r/K_z , determined previously by the Neuman method (average of 4.8 for IFP-1/1 and IFP-1/2 and 29.5 for IFP-9), with the assumption that the distance z_f between the bottom of the aquifer and the fracture is equal to $0.5*H$. The radius of the intersected horizontal fractures is 16 and 4 meters at IFP-1 and IFP-9, respectively.

6. CONNECTIVITY OF FRACTURE NETWORK

Considering a typical hydraulic test in fractured rock, the problem arising when analyzing data is the geometry of the fractures system into which flow occurs. According to fracture density and its distribution, the dimension of flow will vary from 0 to 3. The GRF (Generalized Radial Flow) model generalizes the flow dimension to nonintegral values, while retaining the assumptions of radial flow and homogeneity (Barker, 1988).

The theory considers an n -dimensional radial flow into a homogeneous, confined and isotropic fractured medium, characterized by a hydraulic conductivity K_f and specific storage S_{sf} . This Generalized Flow Model introduces the concept of a fractional “dimension,” n , for the flow, which characterizes the variation law of the flow section according to the distance from the pumping well. Values of n vary from 0 to 3: linear when $n=1$; cylindrical when $n=2$ (this corresponds to the Theis model); and spherical when $n=3$. Parameter n can take on any value, integer or not, indicating the geometrical complexity of the flow.

The results of the interpretation of long-duration pumping tests using this technique are summarized in Table 8. The flow-dimension, even though it is very difficult to interpret, is the parameter which provides information on the connectivity: a well-connected fracture network will have a higher value of flow dimension than a poorly connected fracture system (Black, 1994). The obtained flow dimensions are around 2, suggesting a cylindrical flow to a completed well in an isotropic system. This implies a quite good connectivity of the fracture network. These values also suggest that in this anisotropic fractured rock, the horizontal fracture set (HSFN) is well connected, at the scale of pumping test, to a second sub-vertical fracture set (VSFN). Recent work (Kuusela-Lahtinen et al., 2003) on the evolution of the flow dimension with depth in wells in fractured media also suggest the predominance of dimension $n = 2$ at shallow depths. Nevertheless, according to Barker (1988), the GRF model does not permit the introduction of anisotropy in cases of a non-integer dimension; thus, the vertical anisotropy noted in the previous section cannot be confirmed or disproved by this model. Furthermore, there is no clear relationship between the flow dimension and the number of horizontal conductive fractures intersected by the well (Table 8), the connectivity being ensured by the vertical fractures set.

7. SCALE EFFECT

Various authors have observed that hydraulic conductivity is an apparent function of the scale of the measurement. The usual pattern is for hydraulic conductivity to increase with measurement scale up to the point defining the representative elementary volume, beyond which it is approximately constant over at least several orders of magnitude (Clauser, 1992; Rovey, 1998). Although a few authors (Butler and Healey, 1998) have considered it to be linked to artifacts and bias in small-scale field measurements, Clauser (1992), Neuman (1994) and Sanchez-Villa et al. (1996) link this scale dependence to heterogeneity.

From the data available on the weathered-fractured layer of Maheshwaram aquifer, five different scales of data sets are identified. At the smallest scale of investigation, the interpretation of pumping tests using the double-porosity model can describe the hydraulic

conductivity of the blocks. Slug tests, injection and pumping tests characterize the hydraulic conductivity at the borehole level, while calibration of a numerical model with deterministic continuum conductivities produces an estimate of the same parameter at a higher scale (several kilometers). This classical finite-difference 2D-meshed model was calibrated on transient water-table fluctuations observed during two years using the MARTHE code (Thiéry, 1993). MARTHE is a hydrodynamic modeling code, in transient regime with three-dimensional and/or multi-layer flow in porous media. The resolution method uses finite differences with a regular rectangular grid (in this case, a 53x53 grid of 200x200 meters square meshes). To quantify the dependency of hydraulic conductivity on scale, some length parameter must be associated with each test. In the numerical model, for calibration, the watershed was divided into several zones of equal permeability: the size of these zones is attributed as the length parameter for each calibrated permeability. For the pumping and injection tests, as suggested by Rovey and Cherkauer (1995), the radius of influence R_i can be estimated (accurately enough for the purpose) using a form of the Cooper-Jacob distance-drawdown equation:

$$R_i^2 = \frac{2.25 Tt}{S}$$

For the slug tests, the radius of influence is given by Bouwer and Rice (1976). A scale-effect analysis for hydraulic conductivity of the blocks (K_b), obtained from the double-porosity model, was carried out by the introduction of an arbitrary length of 0.2 meter in order to avoid statistically the secondary fracture network.

The relationship between hydraulic conductivity and scale of measurement (R_i) is plotted on a log-log diagram (Figure 10), along with an outline of the region corresponding to the data trend obtained by Clauser (1992) on a large data set of crystalline rocks. The data for Maheshwaram are located at the upper limit of that general trend (towards the highest permeabilities). This is most probably due to the near-surface origin of these data compared to the deeper origins of the crystalline rocks constituting the total database (data from tunnels, very deep wells, etc.). The impact of weathering-related fracturing in the basin increases the hydraulic conductivity by two orders of magnitude, as compared to the general data. Moreover, for the data from North America, the erosion by Quaternary glaciers of the superficial formations including the weathered-fractured layer contributes to a decrease in the general data trend of Clauser (1992).

As mentioned previously, the hydraulic conductivity increases from matrix (centimeter scale: K_m) to block (decimeter scale: K_b) size due to the contribution of the primary fracture network (PFN). It continues to increase from block scale up to borehole scale (meters to hundreds of meters), as observed in many cases, due to the effect of the horizontal (HSFN) and sub-vertical (VSFN) sets of secondary fracture network. At the borehole scale, the ratio between the average permeability from pumping tests and the average permeability from slug tests for wells tested by pumping tests is 3:1. This same ratio is observed between the average slug-test hydraulic conductivity (1.2×10^{-5} m/s) in wells investigated by long-duration pumping tests and the average slug-test hydraulic conductivity (4.4×10^{-6} m/s) for all wells. This means that the apparent permeability increase is linked to a bias in the pumping-test data, as has been previously noted for the flowmeter data (Figure 5). Thus, at the borehole scale, the hydraulic conductivity does not increase significantly.

Rovey and Cherkauer (1995) explained the increase in permeability from the pumping tests relative to the slug tests by proposing that at small scales the hydraulic conductivity and the groundwater flow (as measured by slug tests) would tend not to be influenced by the rare heterogeneities that increase the conductivity and flow rates over a regional scale (as measured by long duration pumping tests). Stated otherwise, the chances of a small-scale test encountering an extremely rare high-conductivity heterogeneity would be disproportionately

small relative to the degree with which that heterogeneity increases regional hydraulic conductivity. This is not the case in our study area. Reversing Rovey's argument that the greater the heterogeneity the larger the scale effect (Rovey, 1998), the absence of a scale effect in the weathered-fractured layer of Maheshwaram suggests that the hydraulic conductivity at the borehole scale is laterally homogeneous. This is in agreement with the previous results (c.f. §3.) showing the relative homogeneity of the fracture permeability, with the total permeability being controlled mainly by the frequency of medium-conductivity fractures. Finally, the large-scale data from the numerical model MARTHE exhibit a lower variability due to the longer-scale averaging of the parameters.

8. DISCUSSION

The information acquired in the study area introduces a conceptual hydrodynamic model for the weathered-fractured layer of the hard rock aquifers (Figure 11).

Our data show that the weathered-fractured layer is mainly conductive from its upper surface to a depth of 35 meters, within which range conductive fracture zones with transmissivities greater than $5 \times 10^{-6} \text{ m}^2/\text{s}$ are observed. The lower limit corresponds to the top of the fresh basement, which contains few or no highly conductive fractures ($T > 5 \times 10^{-6} \text{ m}^2/\text{s}$) and where only local deep tectonic fractures are hypothesized to be significantly conductive at great depths as observed by studies in Sweden (Talbot and Sirat, 2001), Finland (Elo, 1992) or United States (Stuckless and Dudley, 2002). An unpublished study in the same area has statistically confirmed this result by the analysis of airlift flow rates in 288 boreholes, 10 to 90 meters deep. It is observed that the cumulative airlift flow rate ranges from $1.5 \text{ m}^3/\text{h}$ to $45 \text{ m}^3/\text{h}$ (Figure 12), the mean value increasing drastically in the weathered-fractured layer between 20 and 30 meters deep. Below 30 meters, the flow rate is constant and does not increase with depth. In practice, drilling deeper than the bottom of the weathered-fractured layer (30 – 35 meters) does not increase the probability of improving the well discharge. The data confirm that the weathered-fractured layer is the most productive part of the hard-rock aquifer, as already shown elsewhere by other authors (Houston and Lewis 1988, Taylor and Howard 2000).

Two different scales of fracture networks are identified and characterized by the hydraulic tests: the primary fracture network (PFN) which affects the matrix at the decimeter scale, while secondary fracture network (SFN) affects the blocks at the borehole scale. The latter is described first below.

The secondary network is composed of two conductive fractures sets - a horizontal set (HSFN) and a subvertical set (VSFN) as observed in outcrop. These are the main contributors to the permeability of the weathered-fractured layer. The average vertical density of the horizontal conductive set ranges from 0.15 m^{-1} to 0.24 m^{-1} , with a fracture length of a few tens of meters (10 - 30 meters-diameter for the only available data). This corresponds to a mean vertical thickness of the blocks ranging from 4.17 (≈ 4) to 6.67 (≈ 7) meters. The high dependence of permeability on the density of the conductive fractures indicates that individual fractures contribute more or less equally to the bulk horizontal conductivity ($K_r = 10^{-5} \text{ m/s}$) of the aquifer. No strong heterogeneity is detected in the distribution of the hydraulic conductivities of the fractures, and therefore no scale effect was induced at the borehole scale. The subvertical conductive fracture set connects the horizontal network, insuring a vertical permeability ($K_z = 10^{-6} \text{ m/s}$) and a good connectivity in the aquifer. Nevertheless, the subvertical set of fractures is less permeable than the horizontal, introducing a horizontal-to-vertical anisotropy ratio for the permeability close to 10 due to the supremacy of horizontal fractures.

The existence of a secondary fractures network only in the upper part of the subsurface profile and the relative homogeneity of its characteristics are indicators that a superficial and laterally continuous process is responsible for the origin of the fractures. In the absence of glaciers and conditions favoring high erosion in the study area, another process than decompression must be invoked to explain the genesis of the primary and secondary fractures. Wyns et al. (2004) have shown that fracturing in hard-rock areas depends not only on the decompression processes, but also on the mineral weathering process. The weathering of the micaceous minerals, particularly biotites, to clays proceeds with an increase in volume, which induces cracks in the rock that will initiate fracturing. Where the rock texture is isotropic (e.g., in granite), the fractures are mostly subparallel to the contemporaneous weathering surface, as in the flat Maheshwaram watershed where they are horizontal (Maréchal et al., 2003c). In highly foliated rocks (metamorphic rocks), orientation of fractures can be also controlled by the rock structure (Pye, 1986). Resulting non-horizontal fractures are less affected by the closing effect of lithostatic constraint. This could explain the less rapid vertical decrease in permeability of these rocks compared with granitic rocks as reported by Havlík-Krásný (1998) and Krásný (1999). At a regional (and borehole) scale, the weathering process is much more homogeneous than tectonic phenomena (local deep-fault zones) and corresponds more closely to the observations in our study area. In the field, the borewells that were drilled with a quite homogeneous spacing throughout the watershed confirm this conclusion: of 288 wells, 257 (89%) were drilled deeper than 20 meters and 98% of these are productive. In any case, the probability of a vertical well crossing a horizontal fracture induced by such wide-scale weathering is very high.

The primary network of fractures (PFN), operating at the block scale, increases the original matrix permeability of $K_m = 10^{-14} - 10^{-9}$ m/s to $K_b = 4 \times 10^{-8}$ m/s. Regarding the matrix storage, it also should contribute to the storage coefficient in the blocks of $S_b = 5.7 \times 10^{-3}$. The storage in the blocks represents 91 % of the total specific yield ($S_y = 6.3 \times 10^{-3}$) of the aquifer; storage in the secondary fracture network accounts for the rest. Such a high storage in the blocks (in both the matrix and the PFN) and the generation of the PFN would result from a first stage of the weathering process itself. The development of the SFN would be the second stage in the weathering process: that is why the words “primary” and “secondary” have been chosen to qualify the different levels of fractures networks. The obtained storage values are compatible with those of typical unconfined aquifers in the absence of an impermeable layer confining the aquifer.

9. CONCLUSION

The complementarity of various interpretation techniques specifically designed for fractured media is demonstrated in order to elaborate a comprehensive hydraulic model for an example weathered-fractured zone of a hard rock aquifer. They constitute a useful toolbox for the interpretation of hydraulic tests in fractured hard rocks. A hydrodynamic model of the weathered-fractured layer of the aquifer is proposed based on the values of the properties obtained from hydraulic tests at different scales in the Maheshwaram watershed.

Many geological and hydrogeological indicators suggest that a continuous and laterally homogeneous weathering process is responsible for the origin of the fractures and permeability encountered in the aquifer. These results confirm the major role played by weathering in the origin of the fractures and on the resulting hydrodynamic parameters in shallow hard-rock aquifers.

The universal character of granite weathering and its worldwide distribution underlines the importance of understanding its impact on the hydrodynamic properties of the

aquifers present in these environments. This generic model for permeability and storage in weathered granitic aquifers needs to be tested elsewhere.

Notation

b	initial saturated thickness of aquifer (AN and GRF models, Dupuit solution for injection test), m.
H	thickness of confined aquifer (SF and DP models), m.
H_{DG}	Gringarten dimensionless thickness of the aquifer, $H_{DG} = H/r_f \sqrt{K_r/K_z}$
K_b	hydraulic conductivity of the block medium (DP model), m/s.
K_{CFZ}	hydraulic conductivity of conductive fractures zone, m/s,
K_f	hydraulic conductivity of fracture medium (DP and GRF models), m/s.
K_m	hydraulic conductivity of the matrix, m/s.
K_r	horizontal hydraulic conductivity (AN and SF models), m/s.
K	total hydraulic conductivity (injection and slug tests), m/s.
K_z	vertical hydraulic conductivity (AN and SF models), m/s.
K_D	degree of anisotropy (AN and SF models), equal to K_z / K_r .
l	width of the blocks or persistence (DP model), m.
n	dimension of the fracture flow system (GRF model).
N	number of fractures sets (DP model), $N = 1,2,3$.
Q	pumping rate, m ³ /s.
r	radial distance from pumping well, m.
r_f	fracture radius (DP model), m.
r_w	well radius, m.
R_i	radius of influence, m.
s	drawdown, m.
s_{DG}	Gringarten dimensionless drawdown, equal to $4\pi \sqrt{K_r K_z} r_f s / Q$.
s_{DN}	Neuman dimensionless drawdown, equal to $4\pi T s / S$.
S	(elastic) storage coefficient (AN model), equal to $S_s b$
S_f	storage coefficient (specific yield in unconfined aquifer) of fracture medium (DP model).
S_b	storage coefficient (specific yield in unconfined aquifer) of block medium (DP model).
S_s	specific (elastic) storage, m ⁻¹ .
S_{sf}	specific storage of the fracture fracture system (GRF model), m ⁻¹ .
S_y	specific yield (AN and DP models).
t	time since pumping started, s.
t_s	Neuman dimensionless time with respect to S_s , equal to $Tt / S r^2$.
t_y	Neuman dimensionless time with respect to S_y , equal to $Tt / S_y r^2$.
t_{DG}	Gringarten dimensionless time, $K_r t / S_s r_f^2$
T	transmissivity $K_r b$, m ² /s.
z_f	distance between aquifer bottom and horizontal fracture (SF model), m.
CFZ	conductive fractures zone
PFN	primary fractures network
SFN	secondary fractures network
VSFN	subvertical fractures set of SFN

HSFN horizontal fractures set of SFN

Acknowledgments

This study has been carried out at the Indo-French Center for Groundwater Research (BRGM-NGRI). The authors wish to thank the French Ministry of External Affairs and the Embassy in India Cooperation and Cultural Service for their support and the funding of missions of French scientists. The Indo-French Center for Groundwater Research has also benefited from CNRS funding within the framework of the ACI Program “Water and Environment” and from funding from the IFCPAR (Indo-French Center for the Promotion of Advanced Research). This paper has benefited immensely from the detailed comments and inputs provided by Patrick Lachassagne on various drafts and the research assistance provided by Jean-Baptiste Charlier, Riccardo Torri and Dewashish Kumar.

References

- Acworth, R.I., The development of crystalline basement aquifers in a tropical environment. *Q. J. Eng. Geol.*, 20, 265-272, 1987.
- Barenblatt, G.I. and I.P. Zheltov, Fundamental equations of filtration of homogeneous liquids in fissured rocks, *Soviet Dokl. Akad. Nauk.*, 13(2), 545-548, 1960.
- Barenblatt, G.I., I.P. Zheltov and I.N. Kochina, Basic concepts in the theory of seepage of homogeneous liquids in fissured rocks, *Soviet Appl. Math. Mech.*, 24(5), 852-864, 1960.
- Barker, J.A., A generalized radial flow model for hydraulic tests in fractured rock. *Water Resources Research*, 24(10), 1796-1804, 1988.
- Barker, R.D., C.C. White and J.F.T. Houston, Borehole siting in an African accelerated drought relief project, in *Hydrogeology of crystalline basement aquifers in Africa*, edited by E.P. Wright and W.G. Burgess, pp. 183-201, *Geological Soc. Spec. Publ.*, 66, 1992.
- Bear, J.D., Modeling flow and contaminant transport in fractured rocks, in *Flow and Contaminant Transport in Fractured Rock*, edited by J. Bear, Chin-Fu Tsang and G. de Marsily, pp. 1-37, Academic Press, London, 1993.
- Black, J.H., Hydrogeology of fractured rocks – a question of uncertainty about geometry, *Applied Hydrogeology*, 3, 56-70, 1994.
- Blomqvist, R.G., Deep groundwaters in the crystalline basement of Finland, with implications for nuclear waste disposal studies, *Geologiska Foereningen i Stockholm Foerhandlingar*, 112(4), 369-374, 1990.
- Boulton, N.S., Analysis of data from pumping tests in unconfined anisotropic aquifers, *J. Hydrol.*, 10, 369-378, 1970.
- Boulton, N.S. and J.M.A. Pontin, An extended theory of delayed yield from storage applied to pumping tests in unconfined anisotropic aquifers, *J. Hydrol.*, 14, 53-65, 1971.
- Bouwer, H. and R.C. Rice, A slug test for determining hydraulic conductivity of unconfined aquifers with completely or partially penetrating wells, *Water Resour. Res.*, 12(3), 423-428, 1976.
- Bredehoeft, J.D., The water budget myth revisited: why hydrogeologists model, *Ground Water*, 40(4), 340-345, 2002.
- Butler, J.J. and J.M. Healey, Relationship between pumping-test and slug-test parameters: scale effect or artifact?, *Ground Water*, 36(2), 305-313, 1998.
- Chilton, P.J. and S.S.D. Foster, Hydrogeological characterization and water-supply potential of basement aquifers in tropical Africa, *Hydrogeology J.*, 3(1), 36-49, 1984.
- Chilton, P.J. and A.K. Smith-Carington, Characteristics of the weathered basement aquifer in Malawi in relation to rural water supplies, in *Proc. Challenges in African hydrology and water resources Symp. IAH Series Publ. 144*, pp. 15-23, 1984.
- Clauser, C., Permeability of Crystalline Rocks, *Eos, Transactions, American Geophysical Union*, 73(21), 233-240, 1992
- Davis, S.N. and L.J. Turk, Optimum depth of wells in crystalline rocks, *Ground Water*, 2(2), 6-11, 1964.
- Detay, M., P. Poyet, Y. Emsellem, A. Bernardi and G. Aubrac, Development of the saprolite reservoir and its state of saturation: influence on the hydrodynamic characteristics of drillings in crystalline basement (in French), *C. R. Acad. Sci. Paris II*, 309, 429-436, 1989.
- Dupuit, J., Etudes théoriques et pratiques sur le mouvement des eaux dans les canaux découverts et à travers les terrains perméables, 1st and 2nd Ed. Dunod, Paris, 1848, 1863.
- Elo, S., Geophysical indications of deep fractures in the Narankavaara-Syote and Kandalaksha-Puolanka zones, *Geological Survey of Finland*, 13, 43-50, 1992.

- Foster, S.S.D., African groundwater development – the challenges for hydrological science, *IAHS Publication*, 144, 3-12, 1984.
- Gringarten, A.C. and P.A. Witherspoon, A method of analysing pump test data from fractured aquifers, in *Percolation through fractured rock*, edited by I.A.o.R. Mehan. (Ed.), Deutsche Gesellschaft fur Red and Grundbau, Stuttgart, pp. T3B1-T3B8, 1972.
- Gringarten, A.C. and H.J. Ramey, Unsteady-state pressure distribution created by a well with a single horizontal fracture, partially penetrating or restricted entry, *Trans. Am. Inst. Min. Eng.*, 257, 413-426, 1974.
- Gustafson, G. and J. Krásný, Crystalline rock aquifers: their occurrence, use and importance, *Applied Hydrogeology*, 2, 64-75, 1994.
- Havlík, M. and J. Krásný, Transmissivity Distribution in Southern Part of the Bohemian Massif: Regional Trends and Local Anomalies, *Hardrock Hydrogeology of the Bohemian Massif, Proc. 3rd Internat. Workshop 1998, Windischeschenbach. Münchner Geol. Hefte*, B8, 11-18, 1998.
- Houston, J.F.T. and R.T. Lewis, The Victoria Province drought relief project, II. Borehole yield relationships, *Groundwater*, 26(4), 418-426, 1988.
- Howard, K.W.F., M. Hughes, D.L. Charlesworth and G. Ngobi, Hydrogeologic evaluation of fracture permeability in crystalline basement aquifers of Uganda, *Hydrogeology J.*, 1, 55-65, 1992.
- Jacob, C.E., Drawdown test to determine effective radius of an artesian well, *ASCE Trans.*, 112(232), 1047-1064, 1947.
- Krásný, J., Hard-rock hydrogeology in the Czech Republic, *Hydrogéologie*, 2, 25-38, 1999.
- Kuusela-Lahtinen, A., A. Niemi and A. Luukkonen, Flow dimension as an indicator of hydraulic behavior in site characterization of fractured rock, *Ground Water*, 41(3), 333-341, 2003.
- Lachassagne, P., R. Wyns, P. Bérard, T. Bruel, L. Chéry, T. Coutand, J.F. Desprats, P. Le Strat, Exploitation of high-yield in hard-rock aquifers: Downscaling methodology combining GIS and multicriteria analysis to delineate field prospecting zones, *Ground Water*, 39(4), 568-581, 2001.
- Mabee, S. B. and K. C. Hardcastle, Analysing outcrop-scale fracture features to supplement investigations of bedrock aquifers, *Hydrogeology J.*, 5(3), 82-88, 1997.
- Maréchal, J.C., B. Dewandel, K. Subrahmanyam and R. Torri, Review of Specific Methods for the Evaluation of Hydraulic Properties in Fractured Hard-rock Aquifers, *Current Science of India*, 85(4), 511-516, 2003a.
- Maréchal, J.C., L. Galeazzi, B. Dewandel and S. Ahmed, Importance of irrigation return flow on the groundwater budget of a rural basin in India, in *Hydrology of the Mediterranean and Semiarid Regions*, *IAHS Publ*, 278, 62-67, 2003b.
- Maréchal, J.C., R. Wyns, P. Lachassagne, K. Subrahmanyam and F. Touchard, Anisotropie verticale de la perméabilité de l'horizon fissuré des aquifères de socle : concordance avec la structure géologique des profils d'altération, *C.R. Geoscience*, 335, 451-460, 2003c.
- Marsily, G. de, *Quantitative Hydrogeology*, San Diego, California, Academic Press, 1986.
- Molz F.J., R.H. Morin, A.E. Hess, J.G. Melville and O. Guven, The impeller meter for measuring aquifer permeability variations: evaluation and comparison with other tests, *Water Resour. Res.*, 25(7), 1677-1683, 1989.
- Neuman, S.P., Theory of flow in unconfined aquifers considering delayed response of the water table, *Water Resour. Res.*, 8(4), 1031-1045, 1972.
- Neuman, S.P., Analysis of pumping test data from anisotropic unconfined aquifers considering delayed gravity response, *Water Resour. Res.*, 11(2), 329-342, 1975.
- Neuman, S.P., Generalized scaling of permeabilities: validation and effect of support scale, *Geophysical Research Letters*, 21(5), 349-352, 1994.

- Pickens, J.F., G.E. Grisak, J.D. Avis, D.W. Belanger and M. Thury, Analysis and interpretation of borehole hydraulic tests in deep boreholes; principles, model development, and applications, *Water Resour. Res.*, 23(7), 1341-1375, 1987.
- Pye, K., Mineralogical and textural controls on the weathering of granitoids rocks, *Catena*, 13, 47-57, 1986.
- Rovey, C.W., Digital simulation of the scale effect in hydraulic conductivity, *Hydrogeology J.*, 6, 216-225, 1998.
- Rovey, C.W. and D.S. Cherkauer, Scale dependency of hydraulic conductivity measurements. *Ground Water*, 33(5), 769-780, 1995.
- Sanchez-Vila, X., J. Carrera and J.P. Girardi, Scale effects in transmissivity, *J. Hydrol.*, 183, 1-22, 1996.
- Roy, A. D. and T. Shah, Socio-ecology of groundwater irrigation in India, Intensive Use of Groundwater: Challenges and Opportunities. R. Llamas and E. Custodio. Lisse, A.A. Balkema: 307-335, 2002.
- Sander, P., Water-well siting in hard-rock areas: identifying promising targets using a probabilistic approach, *Hydrogeology J.*, 5(3), 32-43, 1997.
- Stuckless, J.S. and W.W. Dudley, The geohydrologic setting of Yucca Mountain, Nevada, *Applied Geochemistry*, 17(6), 659-682, 2002.
- Summers, W.K., Specific capacities of wells in crystalline rocks, *Ground Water*, 10, 37-47, 1972.
- Talbot, C.J. and M. Sirat, Stress control of hydraulic conductivity in fracture-saturated Swedish bedrock, *Engineering Geology*, 61(2-3), 145-153, 2001.
- Taylor, R. and K. Howard, A tectono-geomorphic model of the hydrogeology of deeply weathered crystalline rock: evidence from Uganda, *Hydrogeology J.*, 8(3), 279-294, 2000.
- Thiéry, D., Modélisation des aquifères complexes - Prise en compte de la zone non saturée et de la salinité. Calcul des intervalles de confiance, *Hydrogéologie*, 1993, 4, 325-336, 1993.
- Walker, D.D., B. Gylling, A. Strom and J.O. Selroos, J.O., Hydrogeologic studies for nuclear-waste disposal in Sweden, *Hydrogeology Journal*, 9(5), 419-431, 2001.
- Warren, J.E. and P.J. Root, The behaviour of naturally fractured reservoirs, *Soc. Petroleum Eng. J.*, 3, 245-255, 1963.
- White, L.D., J.F.T. Houston and R.D. Barker, The Victoria Province drought relief project, I. Geophysical siting of boreholes, *Groundwater*, 26(3), 309-316, 1988.
- Wright, E.P., The hydrogeology of crystalline basement aquifers in Africa, in *Hydrogeology of crystalline basement aquifers in Africa*, edited by E.P. Wright and W.G. Burgess, pp. 1-27, *London Spec Publ*, 66, 1992.
- Wyns, R., J. M. Baltassat, P. Lachassagne, A. Legchenko, J. Vairon and F. Mathieu, Application of SNMR soundings for groundwater reserves mapping in weathered basement rocks (Brittany, France), *Bulletin de la Société Géologique de France*, 175(1), 21-34, 2004.

Figures

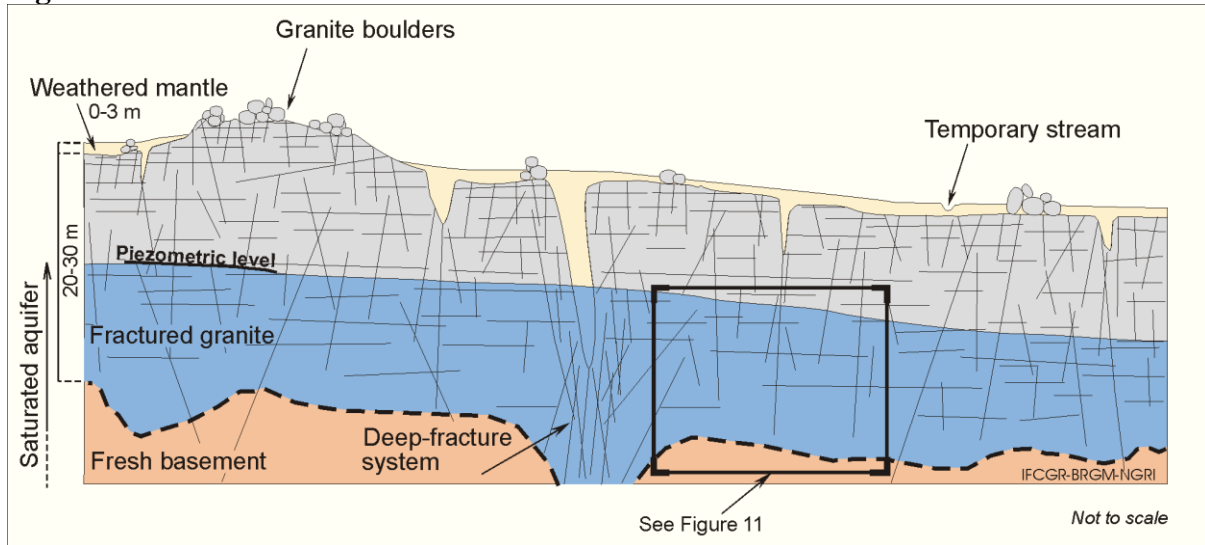


Figure 1. Simplified geological profile of a hard-rock aquifer, modified from Wyns et al. (2004), in accordance with the thickness and geometry of the layers corresponding to the case study.

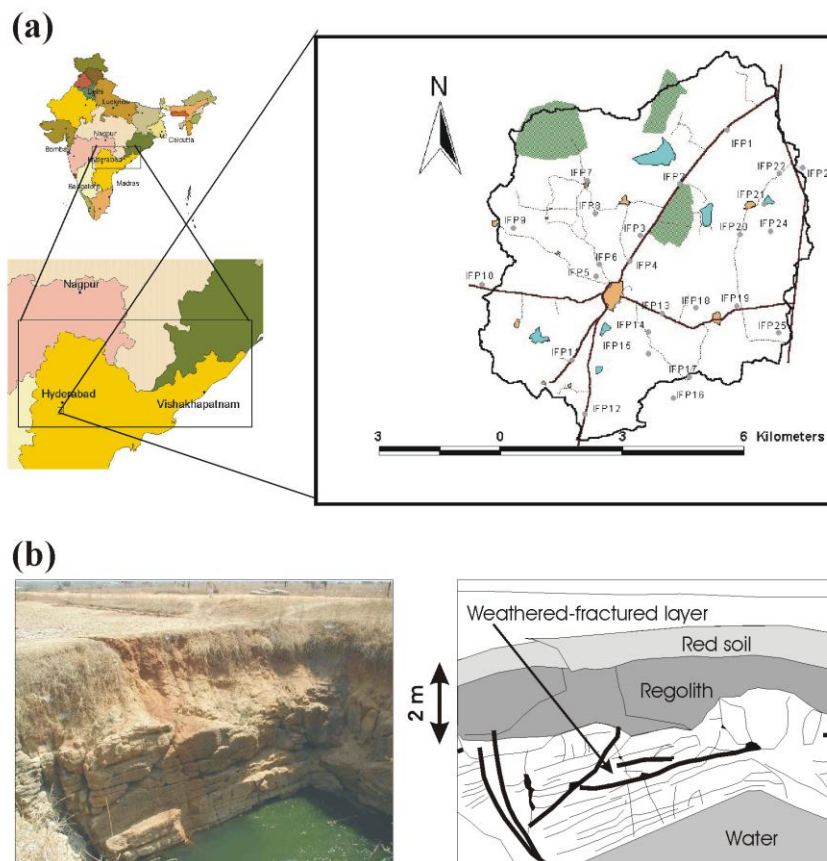


Figure 2. (a) Simplified geology of the study area with locations of the observation wells (IFP-1...25) where the hydraulic tests were conducted (nine additional wells named IFP-1/1, IFP-1/2,...are not located for map clarity reasons). (b) Photograph and geological interpretation of a dugwell in the Maheshwaram area. The horizontal and subvertical fractures networks are visible.

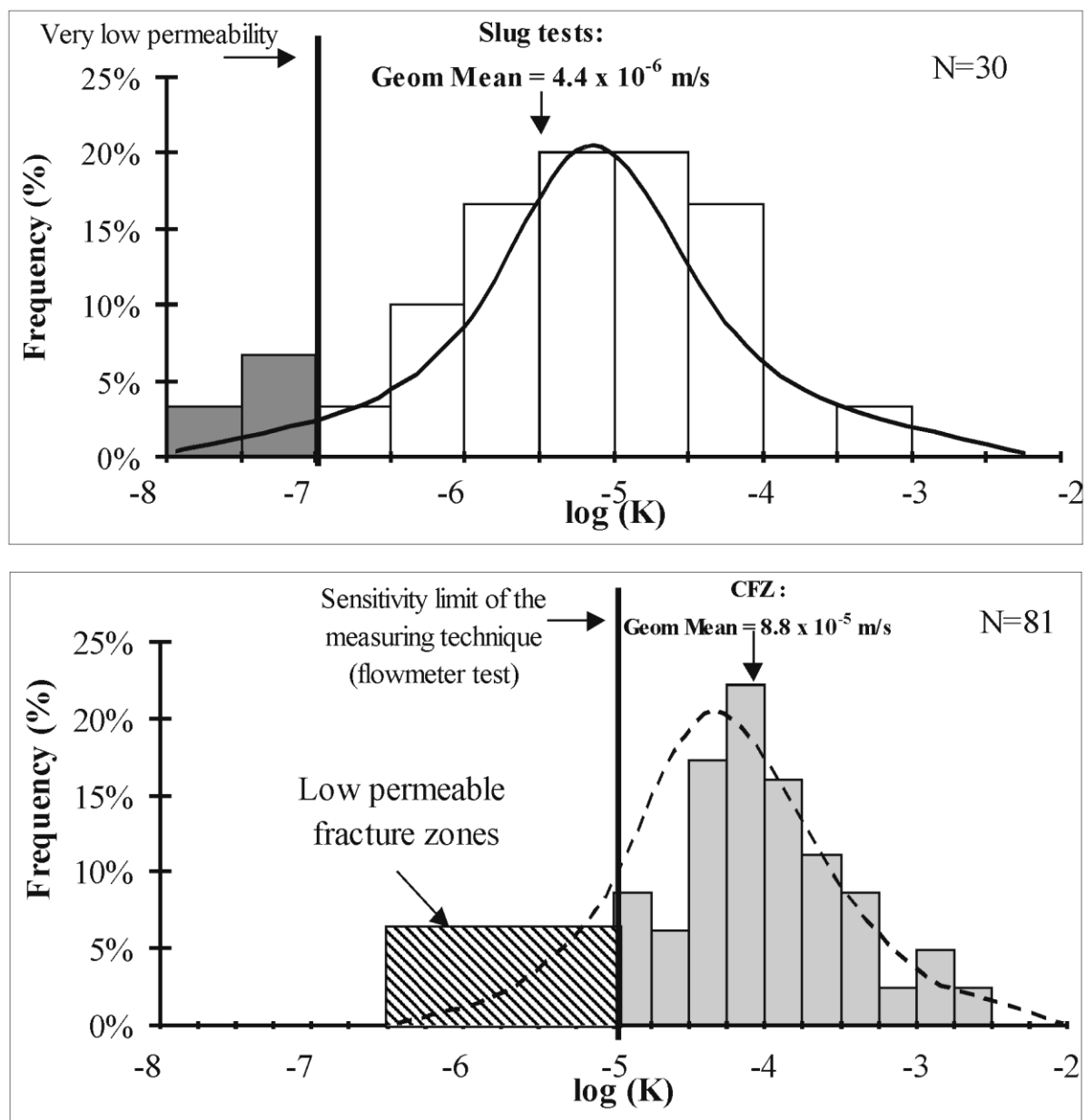


Figure 3. (a) Histograms on a logarithmic scale of the hydraulic conductivity obtained from the slug tests. Lognormal distribution of the permeability includes a population of very low-permeability wells (IFP-5, IFP-19 and IFP-25). (b) Logarithmic histogram of the hydraulic conductivity in 0.5-meter-thick fracture zones obtained from flowmeter injection tests.

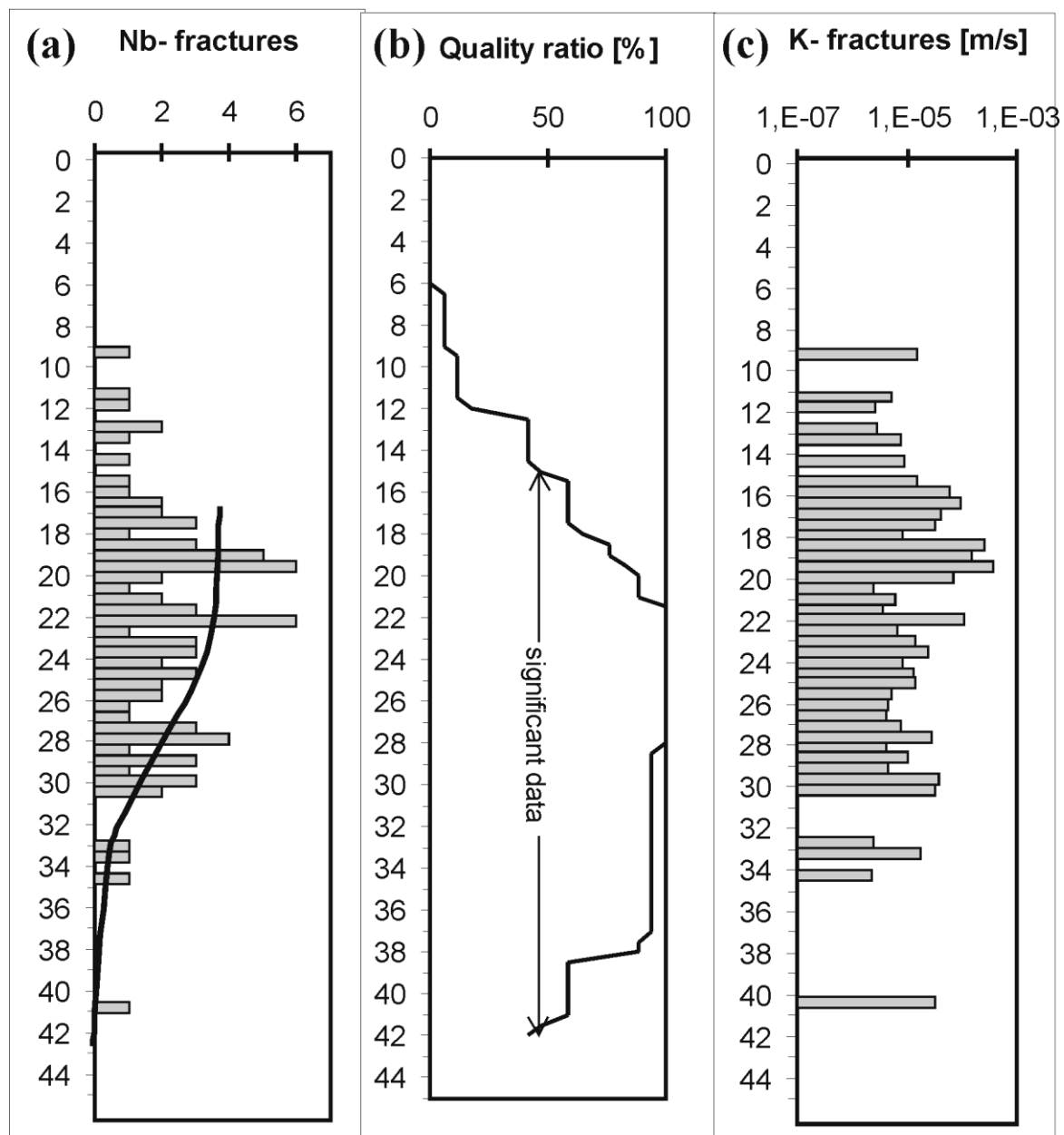


Figure 4. Interpretation of flowmeter-measurement profiles in 0.5-meter-thick layers in the aquifer from 17 wells. (a) The number of hydraulically conductive fractures identified. (b) Quality of observation expressed as the ratio between the number of available observations for each aquifer portion and the total 17 measurements (c) Averages of the fracture permeabilities.

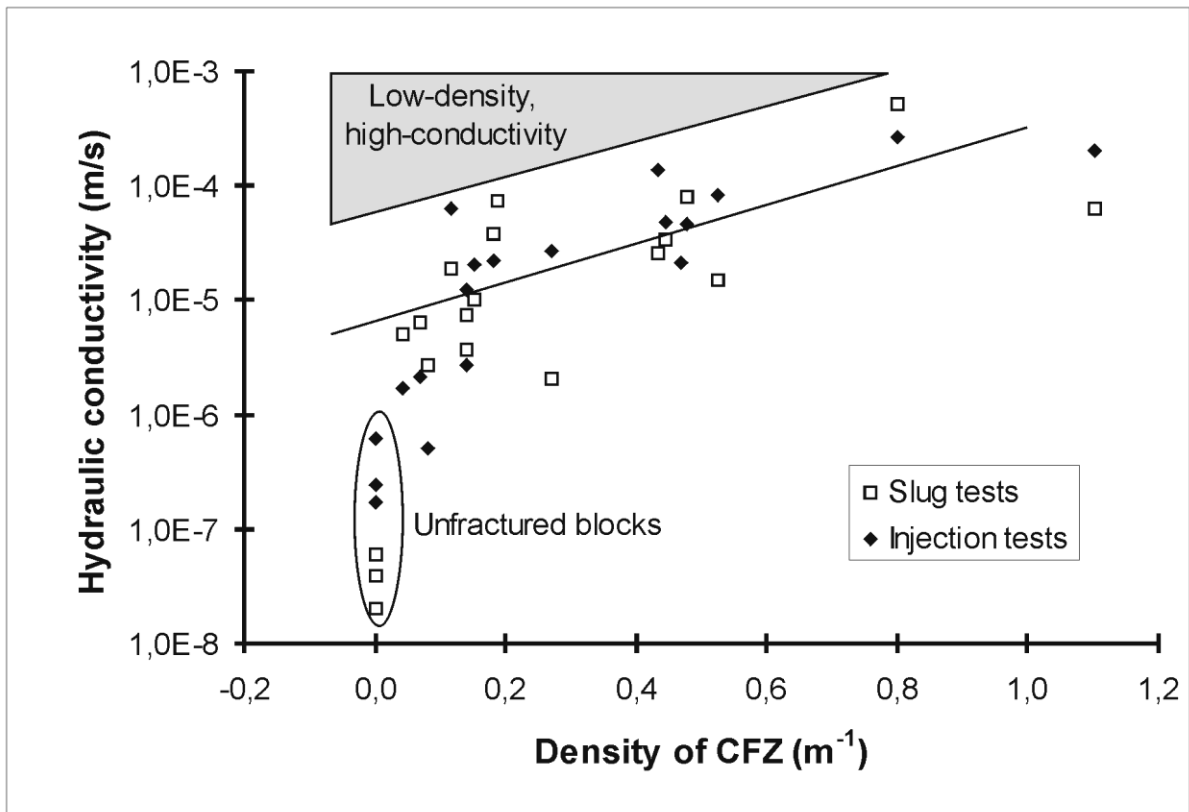


Figure 5. Influence of the density of CFZ (conductive fracture zones) on the hydraulic conductivity at a local scale (slug and injection tests results). The shaded triangle defines the zone of low-density of CFZ with high total hydraulic conductivity.

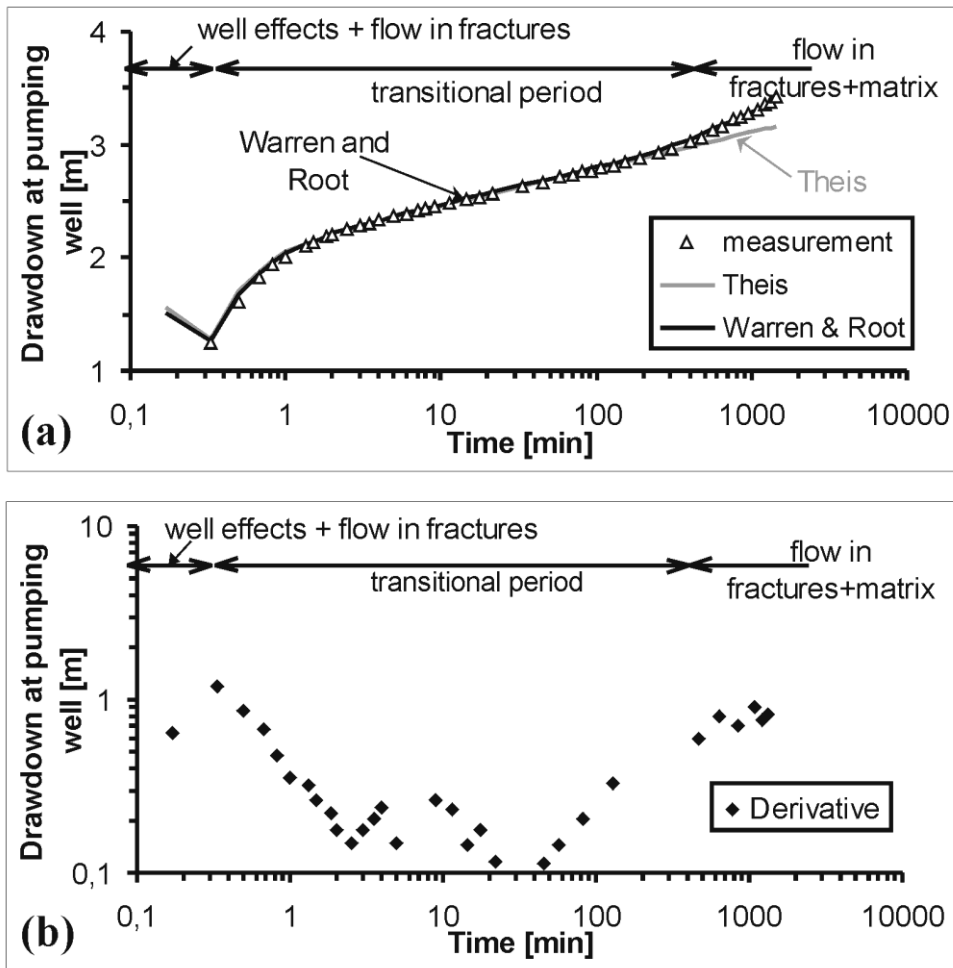


Figure 6. Interpretation at the pumping well IFP-16 using a double-porosity model. (a) Adjustment of drawdown using the Warren and Root double porosity and the Theis methods. (b) 'U'-shape of derivative.

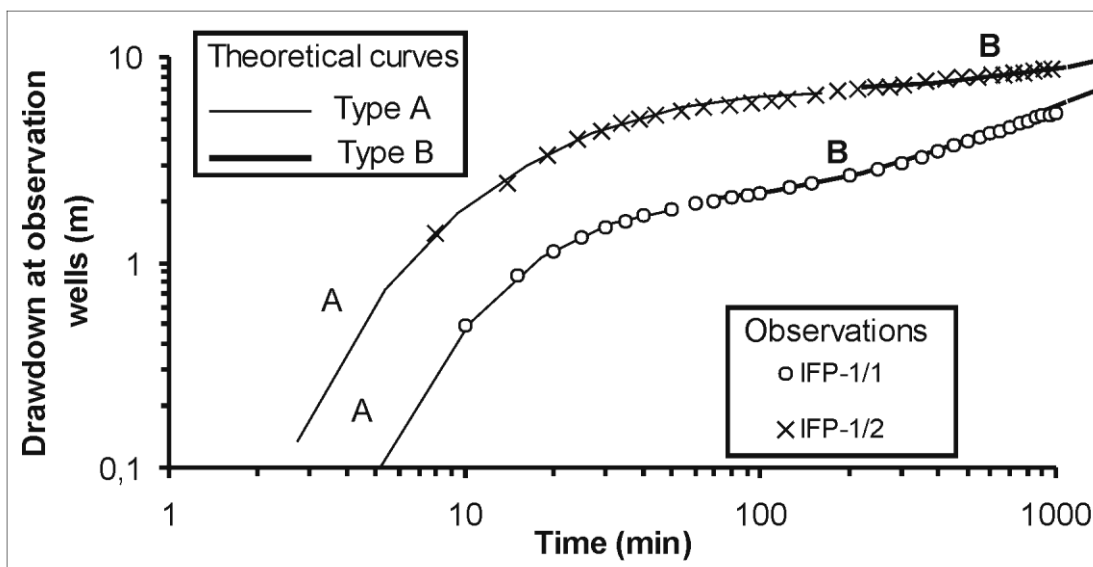


Figure 7. Adjustment of drawdown in observation wells IFP-1/1 and IFP-1/2 using the Neuman (1975) theoretical curves of types A and B.

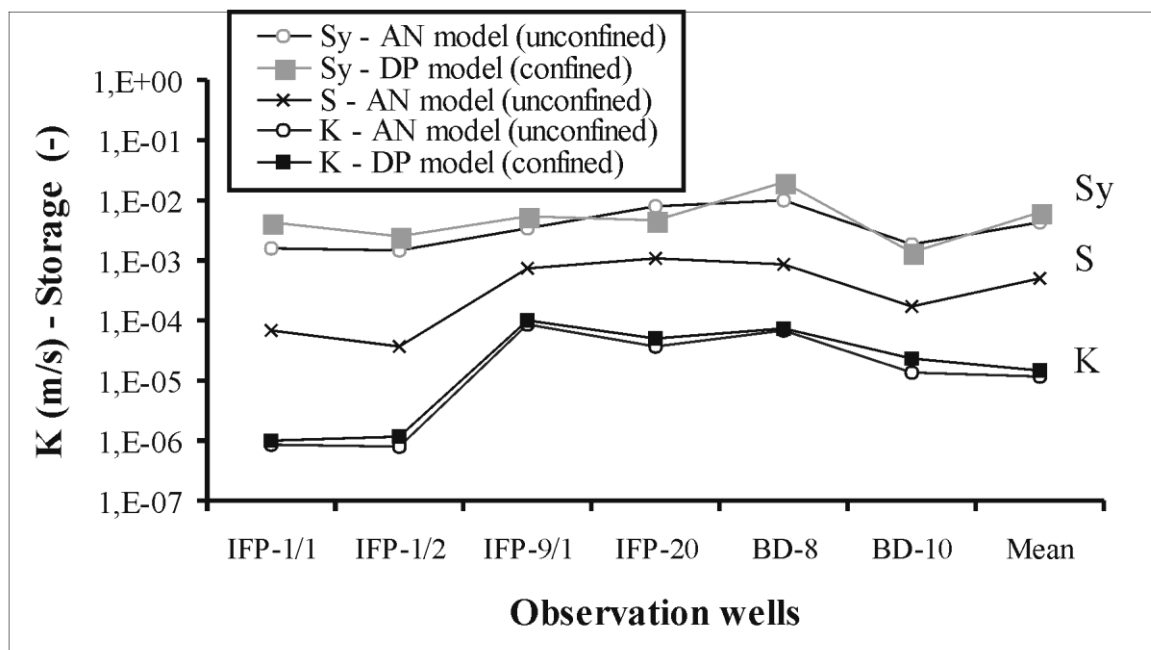


Figure 8. Comparison of storage coefficients and hydraulic conductivities calculated using Double Porosity (DP: confined aquifer solution) and Anisotropic (AN: unconfined aquifer solution) models.

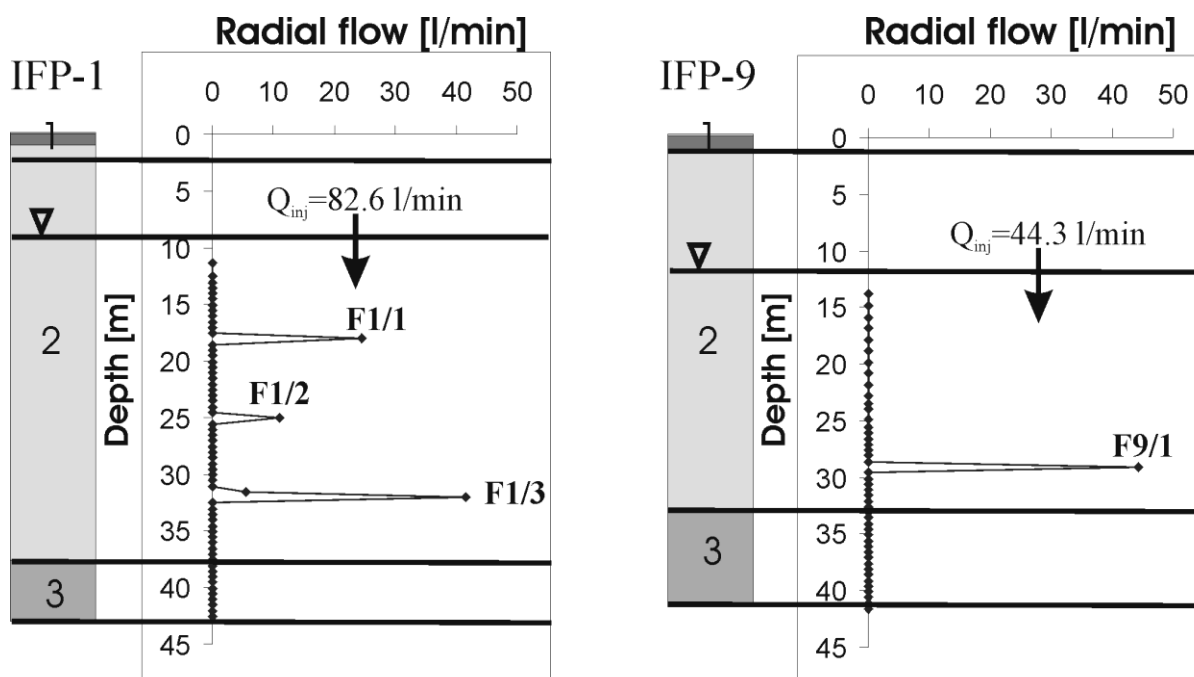


Figure 9. Geological profile of wells IFP-1 and IFP-9 (1, soil and regolith; 2, weathered-fractured layer; 3, fresh basement) and vertical profiles of radial fluxes during an injection test. The conductive fractures are identified. Q_{inj} is the discharge rate during injection and flowmeter tests. The water table indicated on the figure corresponds to the level modified in the well by the injection).

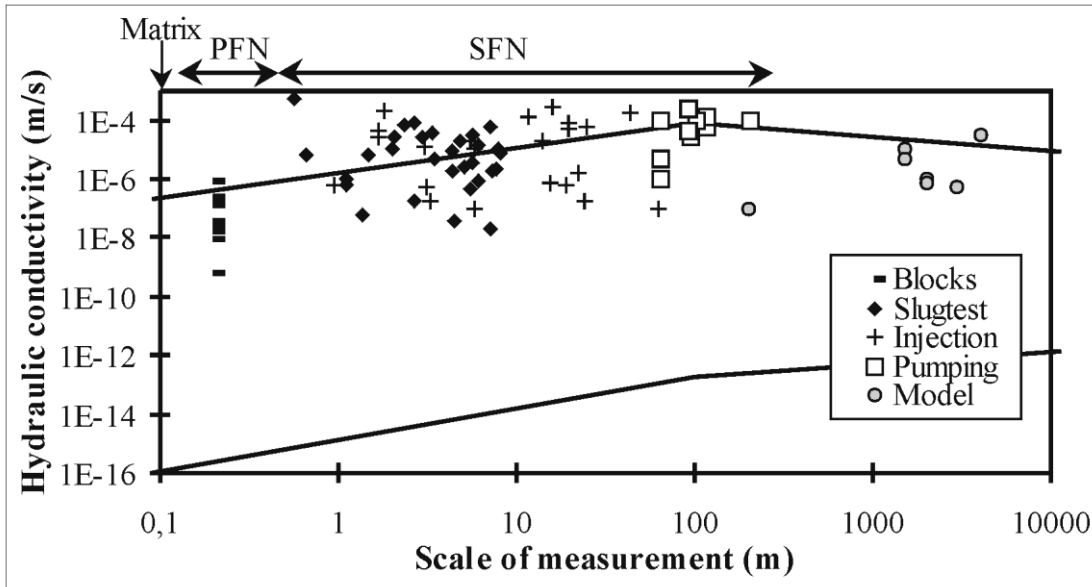


Figure 10. Permeabilities obtained in the study area as a function of the scale of the measurement. The limits of the general data from Clauser (1992) are shown. The permeability increases from the matrix-scale up to the block-scale due to the effects of the primary fracture network (PFN). The secondary fracture network (SFN) contributes to the increase of permeability from block-scale up to hydraulic tests scale.

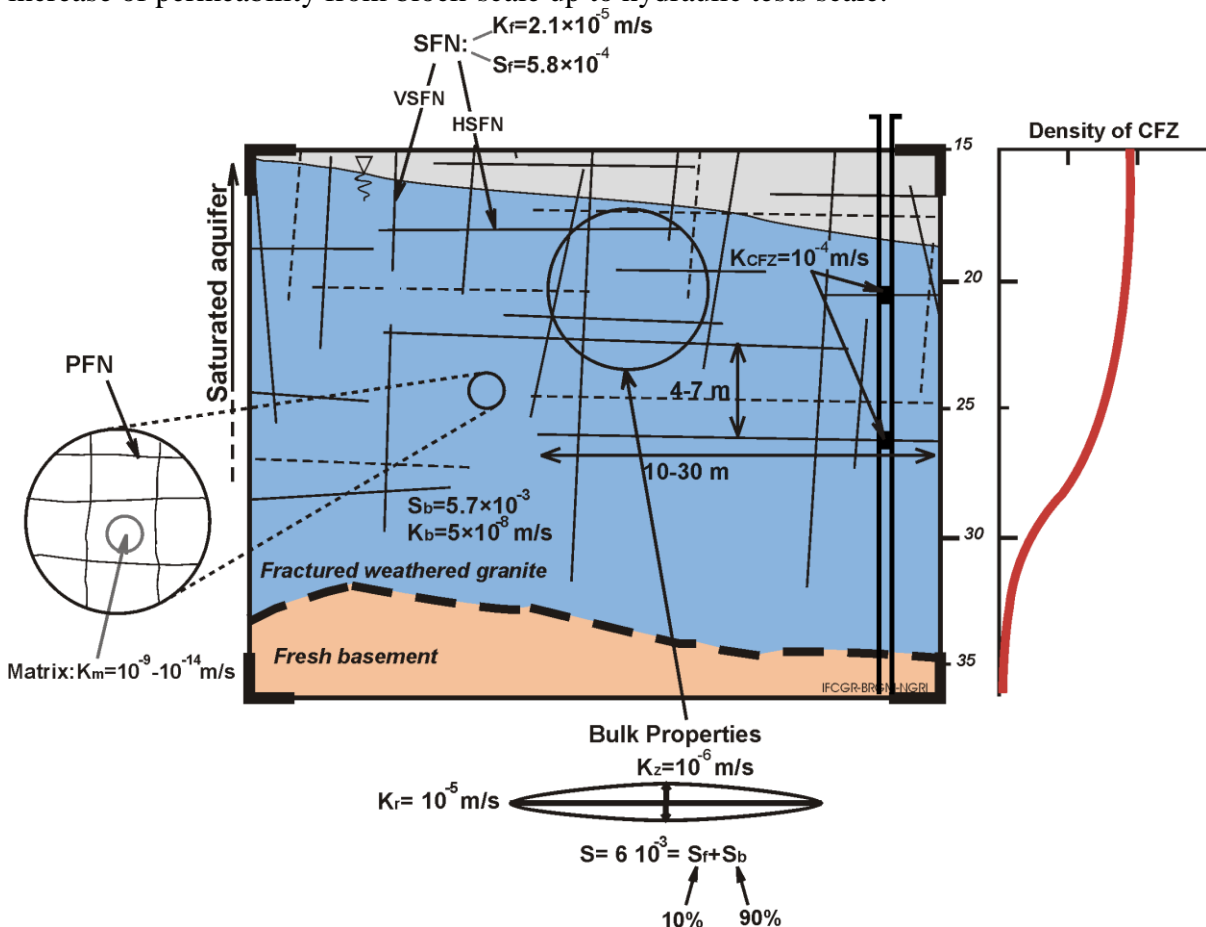


Figure 11. Hydrogeological model of the weathered-fractured layer of the hard-rock aquifer (This figure is a more detailed view of part of the complete weathering profile shown in Figure 1). The dashed lines represent poorly conductive fractures unidentified by the flowmeter tests; solid lines, conductive fractures identified by the flowmeter

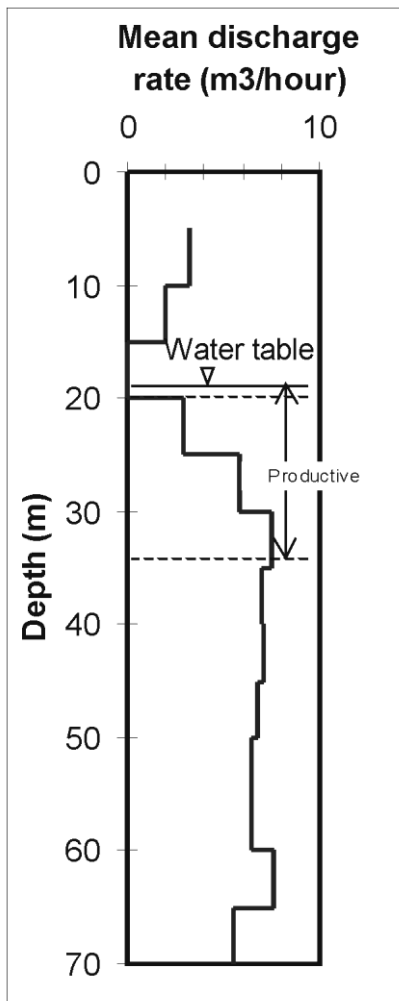


Figure 12: Mean cumulative airlift flow rate versus depth from the 288 wells in the study area. The major increase in flow is located between 20 and 30 meters.

Tables

Hydraulic test	Interpretation method	u/c ¹	t/s ²	Parameters obtained	Scale effect
Slug test	Solution for unconfined aquifers (Bouwer and Rice, 1976)	u	t	Local permeability	
Injection test	Classical Dupuit (1848, 1863) solution	u	s	Permeability	
Flowmeter test	Classical Dupuit (1848, 1863) solution for confined aquifers corrected for unconfined aquifers	u	s	Permeability and density of CFZ ³	
Pumping test	Double porosity (Warren and Root, 1963)	c	t	Bulk permeability and storage of blocks and fractures	
Pumping test	Anisotropy (Neuman, 1975)	u	t	Permeability and storage, degree of permeability anisotropy	
Pumping test	Single fracture (Gringarten, 1974)	c	t	Radius of fractures	
Pumping test	Fractional dimension flow (Barker, 1988)	c	t	Flow dimension, generalized transmissivity and storage	

Table 1. Characteristics of techniques used for the interpretation of hydraulic tests.

¹: hypothesis on aquifer property in the analytical solution (u: unconfined, c: confined)

²: analytical solution type (t: transient, s: steady-state)

³: CFZ: conductive fracture zones (see § 3 for more information)

Well	Depth m	Casing depth m	Water-table depth m	Basement Depth ³ m	K, slug test m/s	K, injection m/s	Number of CFZ ⁴	CFZ density ⁵ m ⁻¹	Persistence ⁶ m
IFP-1	42	8.8	16.7	37.5	7.4E-6	1.3E-5	4	0.14	7.08
IFP-1/1	45	5.75	16.7	35	2.1E-6	n/a ¹	n/a	n/a	n/a
IFP-1/2	35	11.95	18.1	30.2	2.7E-6	5.1E-7	2	0.08	12.29
IFP-1/3	35	5.65	18.5	29	4.4E-7	1.9E-7	u/k ²	u/k	u/k
IFP-2	27.1	0.6	14.8	20	1.9E-7	1.1E-5	u/k	u/k	u/k
IFP-3	37	6.25	11.9	23.5	2.0E-6	2.7E-5	6	0.27	3.71
IFP-4	45	0.8	19	22	6.7E-7	6.0E-7	u/k	u/k	u/k
IFP-5	60	11.65	25.8	36	3.9E-8	1.7E-7	0	0.00	>25.5
IFP-6	42	21.3	21.9	32.2	3.4E-5	4.9E-5	6	0.44	2.25
IFP-7	38	14.8	20.5	18.5	5.1E-4	2.6E-4	3	0.80	1.25
IFP-8	38	12	20.4	22.86	2.6E-5	1.4E-4	5	0.43	2.30
IFP-9	42	12	28.4	33.53	3.8E-5	2.2E-5	4	0.18	5.47
IFP-9/2	42	11.95	28.1	n/a	9.1E-6	n/a	n/a	n/a	n/a
IFP-10	40	1.2	24.7	22	6.4E-6	9.7E-8	u/k	u/k	u/k
IFP-11	42	18.2	21.5	37.5	1.9E-5	6.4E-5	3	0.12	8.62
IFP-11/1	n/a	n/a	21.9	30	n/a	1.6E-5	u/k	u/k	u/k
IFP-11/3	42	19	21.9	35.2	5.0E-6	1.7E-6	1	0.04	23.12
IFP-11/4	39	<12	23.5	28.75	n/a	2.1E-5	5	0.47	2.14
IFP-12	42	21.1	21.0	37.5	3.6E-6	2.7E-6	4	0.14	7.13
IFP-13	50	15.1	23.4	45.73	2.0E-6	n/a	n/a	n/a	n/a
IFP-14	38	15	20.0	23.78	1.0E-5	2.1E-5	3	0.15	6.54
IFP-15	41	12	19.1	23.7	7.3E-5	1.8E-4	2	0.19	5.33
IFP-16	42	14.8	15.2	36.58	6.2E-5	2.0E-4	27	1.10	0.91
IFP-17	38	19.8	18.2	30.48	6.5E-6	2.1E-6	2	0.07	14.71
IFP-18	36.6	16	19.5	22.8	2.9E-5	n/a	n/a	n/a	n/a
IFP-19	41	5.8	13.2	41.14	5.9E-8	6.3E-7	0	0.00	>32.3
IFP-20	41	18.1	19.2	21.1	1.5E-5	8.2E-5	3	0.53	1.90
IFP-21	40	12	13.8	21.1	7.9E-5	4.6E-5	5	0.48	2.09
IFP-22	41	9.7	15.1	41	1.1E-6	9.2E-8	u/k	u/k	u/k
IFP-23	42	13.8	21.2	39	8.8E-7	7.6E-7	u/k	u/k	u/k
IFP-24	49	16.8	18.1	27.5	1.0E-5	1.3E-5	u/k	u/k	u/k
IFP-25	46	5.45	22.5	42	2.0E-8	2.4E-7	0	0	>23.4

Table 2. Characteristics of wells tested by slug and injection.

Notes:

¹n/a = not available for practical reasons,²u/k =: unknown data in low-permeability wells,³according to the geological log, also corresponds to the bottom of the weathered-fractured layer⁴0.5 meter-thick zones;⁵CFZ density is the ratio between the number of conductive fracture zones and the thickness of the investigated part of weathered-fractured layer (equal to the difference between the final water level during the injection test and the bottom of the weathered-fractured layer);⁶persistence, equal to CFZ spacing, is the inverse of density;

K: hydraulic conductivity; CFZ: conductive fracture zones.

Pumping well	Radius r_w m	Observation wells	Pumping rate m^3/s	Duration minutes
IFP-1	0.0825	IFP-1/1 (r = 28 m) IFP-1/2 (r = 27.5 m)	0.0013	1024
IFP-8	0.0825	n/o	0.0017	360
IFP-9	0.0825	IFP-9/1 (r = 30.7 m)	0.0007	720
IFP-16	0.0825	n/o	0.0058	1450
F-20	0.0825	IFP-20 (r = 14.6 m)	0.0009	370
BD-9	0.0825	BD-8 (r = 85 m) BD-10 (r = 50 m)	0.0053	369

Table 3. Characteristics of short- and long-duration pumping tests.

n/o = no observation well

Well	Known parameters		Parameters calculated by adjustment on DP model					
	l m	N	T_f m^2/s	K_f m/s	S_f^2	K_b m/s	S_b^2	S_y^2
IFP-1	7.1	2	6.0E-5	2.8E-6	-	2.6E-8	-	-
IFP-1/1	7.1	1	2.3E-5	1.0E-6	9.0E-4	1.3E-7	3.4E-3	4.3E-3
IFP-1/2	7.1	2	2.6E-5	1.2E-6	1.0E-6	6.9E-10	2.6E-3	2.6E-3
IFP-8	2.3	2	1.2E-3	7.4E-5	-	1.7E-8	-	-
IFP-9	5.5	2	7.6E-4	1.0E-4	-	9.6E-9	-	-
IFP-9/1	5.5	2	7.3E-4	1.0E-4	3.0E-4	8.2E-7	5.0E-3	5.3E-3
IFP-16	0.9	2	1.4E-3	5.9E-5	-	2.6E-7	-	-
IFP-20	1.9	2	9.2E-4	5.1E-5	1.0E-4	3.9E-8	4.4E-3	4.5E-3
BD-8	2.4	2	1.8E-3	7.5E-5	2.0E-3	2.1E-7	1.8E-2	2.0E-2
BD-10	2.4	2	5.6E-4	2.3E-5	2.0E-4	1.7E-7	1.2E-3	1.4E-3
Mean ¹	3.7	-	3.5E-4	2.1E-5	5.8E-4	5.1E-8	5.7E-3	6.3E-3

Table 4. Values of matrix and fracture media hydrodynamic properties calculated using the double-porosity (DP) model

¹arithmetic mean for storage and geometric mean for hydraulic conductivity² S_b , S_f , and S_y : blocks, fractures and total storage coefficients ($S_y = S_b + S_f$), corresponding, in unconfined aquifer, to specific yields

Observation well	Known parameters		Parameters calculated by adjustment on AN model					
	Pumping well	r m	T_A^1 m^2/s	T_B^2 m^2/s	T_A/T_B	T_{AB}^3 m^2/s	S	S_y
IFP-1/1	IFP-1	28	1.8E-5	2.0E-5	0.90	1.9E-5	7.0E-5	1.6E-3
IFP-1/2	IFP-1	27.5	1.7E-5	1.8E-5	0.97	1.7E-5	3.7E-5	1.5E-3
IFP-9/1	IFP-9	30.7	5.5E-4	7.7E-4	0.73	6.5E-4	7.1E-4	3.4E-3
IFP-20	IFP-20F	14.6	6.5E-4	6.9E-4	0.90	6.7E-4	1.1E-3	7.8E-3
BD-8	BD9	85	1.6E-3	1.8E-3	0.90	1.7E-3	8.3E-4	9.7E-3

BD-10	BD9	50	3.2E-4	3.5E-4	0.90	3.4E-4	1.7E-4	1.9E-3
Mean ⁴	-	-	1.9E-4	2.2E-4	0.88	2.1E-4	4.8E-4	4.3E-3

Table 5. Transmissivity and storage parameters obtained by adjusting the drawdown using the anisotropic (AN) model.

¹ T_A : transmissivity obtained by adjustment on type A curve;

² T_B : transmissivity obtained by adjustment on type B curve;

³ T_{AB} : average of T_A and T_B);

⁴arithmetic mean for storage and geometric mean for hydraulic conductivity

Observation well	Known parameters		Parameters calculated by adjustment on SF model				
	r m	b m	β	K_r m/s	K_z m/s	K_D	$1/K_D$
IFP-1/1	28	21.8	1.0	8.5E-7	5.2E-7	0.61	1.7
IFP-1/2	27.5	21.8	0.2	8.0E-7	1.0E-7	0.123	8.0
IFP-9/1	30.7	7.3	0.6	8.9E-5	3.0E-6	0.03	29.5
IFP-20	14.6	18	0.1	3.7E-5	5.6E-6	0.15	6.6
BD-8	85	23.9	0.8	7.0E-5	4.4E-6	0.06	15.8
BD-10	50	23.9	0.4	1.4E-5	1.3E-6	0.09	10.9
Mean ¹	-	-	-	1.1E-5	1.3E-6	0.1	8.7

Table 6. Permeability and degree of anisotropy determined at the observation wells using anisotropic (AN) model.

¹geometric mean.

Pumping Well	Known parameters				Parameters calculated by adjustment on SF model					
	H m	Fracture	z_f m	z_f/H	S_s m^{-1}	H_{DG}	r_f m	K_r m/s	K_z m/s	K_r/K_z
IFP-1	21.8	F1/3	6.0	0.28	-	3	15.9	3.4E-6	7.1E-7	4.8
IFP-9	7.3	F9/1	4.0	0.55	-	10	4.0	5.7E-5	1.9E-6	29.6

Table 7. Permeability, degree of anisotropy and radius of the horizontal fractures determined at pumping wells using the single-fracture (SF) model.

	Known parameters			Parameters calculated by adjustment on GRF model				
	r m	b m	Nr. of CFZ ²	n	K_f m/s	S_{sf} m^{-1}	Kfb^{3-n} $m^{4-n} s^{-1}$	$S_{sf}b^{3-n}$ m^{2-n}
IFP-1	0.0825	21.8	4	2.2	5.0E-6	-	5.9E-5	-
IFP-1/1	28	21.8	-	1.2	9.5E-5	1.2E-5	2.5E-2	3.1E-3
IFP-1/2	30	21.8	2	2.5	9.5E-7	1.0E-6	4.4E-6	4.7E-6
IFP-8	0.0825	15.6	4	2.2	2.9E-5	-	2.6E-4	-
IFP-9	0.0825	7.3	4	2.5	6.2E-5	-	1.7E-4	-

IFP-9/1	30.65	7.3	-	2.0	1.4E-4	3.1E-4	1.0E-3	2.3E-3
IFP-16	0.0825	23.4	13	1.9	9.5E-5	-	3.2E-3	-
IFP-20	14.6	18.0	2	1.9	9.2E-5	7.1E-5	2.2E-3	1.7E-3
BD-8	85	23.9	-	2.0	2.6E-4	8.7E-5	6.3E-3	2.2E-3
BD-10	50	23.9	-	2.0	4.6E-5	1.4E-5	1.2E-3	3.7E-4
Mean ¹			3.9	2.0	4.0E-5	8.3E-5	6.6E-4	1.5E-3

Table 8. Hydrodynamic properties obtained from the interpretation of pumping tests using the Generalized Radial Flow (GRF) model.

¹arithmetic mean for storage and geometric mean for hydraulic conductivity

²inferior or equal to the number of CFZ in Table 2 because less fractures are investigated through pumping tests (water table drawdown desaturating CFZ) than through injection tests (water table increase saturating new CFZ)